Antagonistic negative and positive neurons of the basolateral amygdala

Joshua Kim[1], Michele Pignatelli[1], Sangyu Xu[1], Shigeyoshi Itohara[2] & Susumu Tonegawa[1–3]

The basolateral amygdala (BLA) is a site of convergence of negative and positive stimuli and is critical for emotional behaviors and associations. However, the neural substrate for negative and positive behaviors and relationship between negative and positive representations in the basolateral amygdala are unknown. Here we identify two genetically distinct, spatially segregated populations of excitatory neurons in the mouse BLA that participate in valence-specific behaviors and are connected through mutual inhibition. These results identify a genetically defined neural circuit for the antagonistic control of emotional behaviors and memories.

The basolateral complex of the amygdala consists of two intimately juxtaposed nuclei: the lateral nucleus and basolateral nucleus (BLA)[1,2]. The BLA is a cortex-like brain structure consisting of two types of nonlaminarly organized excitatory pyramidal neurons, magnocellular and parvocellular, segregated respectively into the anterior and posterior BLA (aBLA, pBLA) and intermingled with populations of genetically defined interneurons[1,3–8]. The BLA is activated by negative and positive emotional stimuli and participates in emotional behaviors and associations[9–16]. Recent studies showed that BLA neurons drive opposing behaviors; therefore, the BLA may be a key site for the regulation of negative and positive behaviors[9,15]. Despite the critical role of the BLA in emotional behaviors, it is not established whether the BLA pyramidal neurons that contribute to negative and positive behaviors (negative neurons and positive neurons) are structurally distinct, let alone genetically distinguishable[17,18]. Furthermore, a neural circuit subserving the antagonistic nature of emotional behaviors has yet to be identified.

Recent studies demonstrated that BLA neurons, which express the activity-dependent gene *Fos* during a negative or positive stimulus, are capable of driving a behavioral response consistent with the valence of the experience[9,15]. Therefore, we reasoned that molecular profiles of the putative negative and positive neurons in the BLA could be obtained by using a *Fos*-based genetic expression system. Activity-dependent molecular profiles of BLA neurons may reveal genetic markers unique to negative and positive neurons. In turn, the identification of distinguishing genetic markers for negative and positive BLA neurons will provide a foundation for identifying the neural circuits underlying antagonistic behaviors elicited by negative and positive stimuli.

RESULTS

Identification of BLA genetic markers

Genetics-based RNA profiling strategies in mammalian models have involved ectopically expressing epitope-tagged RNA-associated proteins or exploiting molecular modifications of RNA-associated substrates[19–22]. To obtain transcriptional profiles, we implemented a strategy involving ectopically expressing an epitope-tagged RNA binding protein, poly(A)-binding protein with a C-terminal Flag tag (PABP-Flag)[23]. Two AAV_9 constructs were used, one containing the tetracycline-based transcription factor tTA under the control of the activity-dependent promoter of *Fos* (AAV_9-Fos-tTA) and the other containing *Pabpc1-Flag* under the control of the tetracycline response element *TRE* (AAV_9-TRE-Pabpc1-Flag). Activation of the *Fos* promoter drives the expression of tTA. In the absence of doxycycline (Dox), tTA binds *TRE* to induce the expression of PABP-Flag. PABP-Flag competes with endogenous PABP and binds the poly(A) tails of mRNA, which then can be isolated via immunoprecipitation using an anti-Flag antibody and protein A/G–coated magnetic beads (**Fig. 1a**).

The putative negative and positive neurons were targeted by exposing male mice to footshocks and a female mouse, respectively. AAV_9-Fos-tTA and AAV_9-TRE-Pabpc1-Flag were introduced into the BLA in mice kept on a Dox diet. Once removed from the Dox diet for 2 d, mice were exposed to footshocks or a female mouse, then immediately placed back on a Dox diet for 2 d before sacrifice. Similar numbers of BLA neurons were Flag+ in the shock and female groups; these numbers were greater than those in mice that were kept in their home cages or kept on a Dox diet (**Fig. 1b–e,g–j**). In contrast, more BLA neurons were Flag+ in the mice that underwent kainic acid–induced seizures compare to the shock or female group (**Fig. 1b,f–j**). This affirms the activity dependency of the genetic system. Therefore, we performed RNA immunoprecipitation using antibodies against Flag from the shock and female groups. Isolated RNA was reverse-transcribed to cDNA and underwent microarray analysis using an Affymetrix Mouse 430A chip. After robust multi-array average (RMA) or Affymetrix Microarray Suite 5 (MAS5) normalization (Online Methods), differential gene expression profiles were compared between the shock and female group and were used as the basis of the screen for identifying genetic markers for the putative negative and positive neurons of the BLA (**Fig. 1k** and **Supplementary Fig. 1**).

[1]RIKEN-MIT Center for Neural Circuit Genetics at the Picower Institute for Learning and Memory, Department of Biology and Department of Brain and Cognitive Sciences, Massachusetts Institute of Technology, Cambridge, Massachusetts, USA. [2]Brain Science Institute, RIKEN, Saitama, Japan. [3]Howard Hughes Medical Institute, Massachusetts Institute of Technology, Cambridge, Massachusetts, USA. Correspondence should be addressed to S.T. (tonegawa@mit.edu).
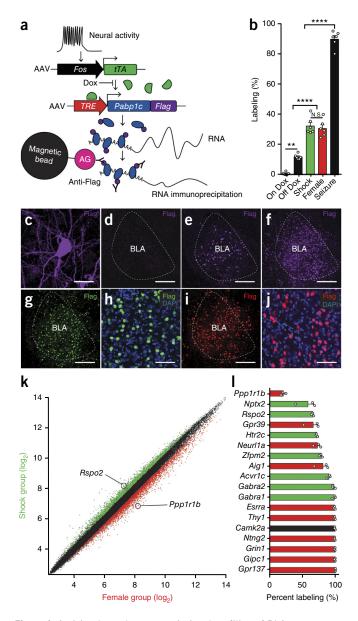
Figure 1 Activity-dependent transcriptional profiling of BLA neurons. (**a**) Viral-based genetic scheme for activity-dependent transcriptional profiling. *Fos* promoter activity drives the expression of tTA, which in turn binds *TRE* and drives the expression of PABP-Flag in the absence of doxycycline (Dox), RNA immunoprecipitated using anti-Flag antibodies and Protein A/G–coated beads. (**b**) PABP-Flag expression in the BLA in mice kept on a Dox diet (On Dox) or taken off a Dox diet and exposed to home cage (Off Dox), shock, female, or seizure (one-way ANOVA, $F_{4,25} = 131.0$, $P < 0.0001$, $n = 6$ per group). Significance for multiple comparisons, $**P = 0.0016$, $****P < 0.0001$; not significant, N.S. ($P = 0.9948$). (**c**) PABP-Flag expression in soma and varicosities of a BLA neuron. (**d**–**j**) Flag expression in the BLA of On Dox (**d**), Off Dox (**e**), seizure (**f**), shock (**g**,**h**), and female-exposed (**i**,**j**) groups. Flag expression and nuclear marker (DAPI) are shown for the shock (**h**) and female (**j**) groups. Scale bars: 25 μm (**c**), 250 μm (**d**–**g**,**i**), 80 μm (**h**,**j**). (**k**) RMA-normalized RNA expression values from microarray analysis of RNA purified from shock ($n = 3$) and female ($n = 3$) groups. Red and green points represent enriched genes (>1.25 fold, ANOVA $P < 0.05$, $\log_2$ scale). (**l**) Quantification of *in situ* hybridization of BLA expression of candidate genetic markers enriched in shock group (green) and female group (red) ($n = 3$ mice per group); black, positive control genes. Results show mean ± s.e.m. (**b**,**l**).

On the basis of previous observations[9,15], we hypothesized that the putative negative and positive BLA neurons would be non-overlapping; therefore, we sought to select from our potential list of candidate genetic markers a single gene candidate, one for each of the putative negative and positive neuron populations. As a corollary, this posits that each of the gene markers would label a subpopulation (<100%) of BLA principal neurons. First, independently of statistical significance, hundreds of genes whose expression was enriched in the shock and female groups were individually screened on Allen Mouse Brain Atlas[24]. We selected 37 genes for single-label fluorescence *in situ* hybridization, of which 16 probes yielded a quantifiable signals in the −1.0 mm to −1.6 mm anterior-posterior (AP) plane of the BLA (**Supplementary Fig. 2**). Quantification of gene expression in the BLA revealed that the majority of these candidate genes were expressed in a virtually all BLA neurons (**Fig. 1l** and **Supplementary Fig. 2**). *Rspo2* (R-spondin 2) was enriched in the shock group (**Fig. 1k**) and was expressed in less than 100% of BLA neurons (**Fig. 1l**). Furthermore, *Rspo2* expression was specific to the BLA, with little expression in other brain areas. In fact, because of this BLA-specific expression, we had previously generated a BLA-restricted Cre transgenic mouse line using the *Rspo2* gene promoter, although we had not further characterized this transgenic mouse with respect to more detailed expression pattern of Cre within the BLA, nor examined the role of *Rspo2*-expressing BLA neurons in valence-related behavior. Therefore, we selected *Rspo2* as a candidate for a negative BLA neuron marker for further anatomical and functional studies of negative BLA neurons. *Rspo2*+ BLA neurons constituted less than 100%, but greater than 50%, of BLA neurons. Among the candidate genes belonging to the female-exposed group, *Ppp1r1b* (protein phosphatase 1 regulatory inhibitor subunit 1B, which encodes DARPP-32)[25] was the only gene that labeled less than 50% of BLA neurons. Furthermore, on the basis of the distribution pattern of *Rspo2* and *Ppp1r1b*, it appeared that these two markers may be expressed in sets of neurons that are non-overlapping. Therefore, we selected *Ppp1r1b* as a potential marker for positive BLA neurons for further characterization.

Double-label single-molecule fluorescence *in situ* hybridization (smFISH) and quantification across the AP axis of the BLA (−0.8 to −2.8 mm from bregma) revealed that *Rspo2* and *Ppp1r1b* labeled spatially segregated population of neurons (**Fig. 2a**–**c**). Less than 1% of BLA neurons were *Rspo2*+*Ppp1r1b*+ (**Table 1**). *Rspo2*+ and *Ppp1r1b*+ BLA neurons were colabeled with the pyramidal neuron marker *Camk2a* and non-overlapping with the inhibitory neuron marker *Gad1* (**Fig. 2d**–**g** and **Table 1**). *Rspo2*+ neurons corresponded to magnocellular pyramidal neurons of the aBLA. In contrast, Ppp1r1b+ neurons corresponded to the parvocellular pyramidal neurons of the pBLA[1,26]. Double smFISH with a *Camk2a* probe and the combined probes for both the *Rspo2* and *Ppp1r1b* showed that virtually all *Camk2a*+ BLA neurons expressed either *Rspo2* or *Ppp1r1b* (**Table 1** and **Supplementary Fig. 3**). Therefore, *Rspo2*+ and *Ppp1r1b*+ neurons collectively define the entirety of BLA pyramidal neurons.
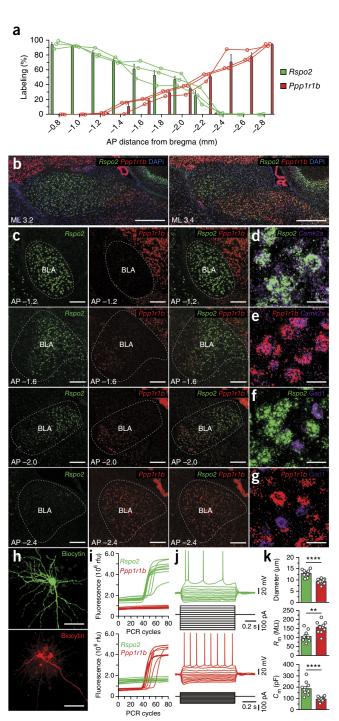
The electrophysiological and morphological properties of *Rspo2*+ and *Ppp1r1b*+ neurons were examined using patch clamp recordings. *Rspo2*+ and *Ppp1r1b*+ were targeted by patching magnocellular and parvocellular BLA neurons, respectively (**Fig. 2h**). To ascertain genetic identity, *Rspo2*+ and *Ppp1r1b*+ neurons were identified by the use of single-cell quantitative PCR (qPCR) from cytoplasmic harvest of patch-clamped recorded BLA neurons. Of 37 magnocellular neurons, single-cell qPCR yielded 10 *Rspo2*+ and 0 *Ppp1r1b*+ neurons; of 38 parvocellular neurons, single-cell qPCR yielded 0 *Rspo2*+ and 11 *Ppp1r1b*+ neurons (**Fig. 2i**). Soma diameter was larger in *Rspo2*+ neurons than *Ppp1r1b*+ neurons; membrane resistance was smaller in *Rspo2*+ neurons than *Ppp1r1b*+ neurons; membrane capacitance was

larger in *Rspo2*^{+} neurons than *Ppp1r1b*^{+} neurons (**Fig. 2j,k**). qPCR-confirmed *Rspo2*^{+} and *Ppp1r1b*^{+} neurons were not significantly different from unconfirmed magnocellular and parvocellular neurons, respectively (**Table 1**). Taken together, then, *Rspo2*^{+} and *Ppp1r1b*^{+} BLA neurons defined spatially segregated, genetically, morphologically, and electrophysiologically distinct cell types.

BLA activation by valence-specific stimuli

If *Rspo2*^{+} and *Ppp1r1b*^{+} neurons represent negative and positive neurons of the BLA, respectively, then stimuli that elicit valence-specific behaviors may differentially activate the aBLA and pBLA. Mice were exposed to the stimuli used to identify BLA gene markers—shocks or female mice—and were sacrificed 90 min later. c-Fos^{+} neurons were quantified separately in the aBLA and pBLA (defined by cytoarchitectural boundaries) by measuring the total number of c-Fos^{+} neurons per section at intervals across the AP axis (**Fig. 3a–c** and **Supplementary Fig. 4**). The relative c-Fos expression, measured by the number of c-Fos^{+} neurons in the aBLA or pBLA as a percentage of total c-Fos^{+} BLA neurons, was significantly greater in the aBLA in response to footshocks compared to exposure to a female mouse or control conditions that delivered no stimulus in a context (**Fig. 3d**). Conversely, relative c-Fos expression was significantly greater in the pBLA in response to female mice compared to exposure shock or control conditions of a neutral context (**Fig. 3d**). In response to valence-specific olfactory stimuli—2,3,5-trimethyl-3-thiazoline (TMT) or peanut oil—relative c-Fos expression was significantly greater in the aBLA in response to TMT compared to exposure to the neutral odor benzaldehyde or peanut oil, while relative c-Fos expression was significantly greater in the pBLA in response to peanut oil compared to exposure to benzaldehyde or TMT (**Fig. 3e**). In response to valence-specific gustatory stimuli —quinine (bitter), water, sucrose (sweet)—relative c-Fos expression was significantly greater in the pBLA in response to water and sucrose water compared to mice that received no water or quinine water (**Fig. 3f**). In contrast, no significant difference was observed in relative c-Fos expression between exposure to quinine water (which elicited little water drinking) compared to no water, as well as between sucrose water and water (**Fig. 3f**). Overall, the aBLA is recruited by stimuli that elicits negative behaviors (shocks, TMT), while the pBLA is recruited by stimuli that elicits positive behaviors (female, water, sucrose, peanut oil).

Double smFISH was performed to directly assess the expression of *Fos* in *Rspo2*^{+} or *Ppp1r1b*^{+} BLA neurons in response to valence-specific stimuli (to be used in subsequent behavioral experiments). Shocks significantly increased *Fos* expression in *Rspo2*^{+} (**Fig. 3g,k**) but not in *Ppp1r1b*^{+} neurons (**Fig. 3h,l**), compared to context (**Fig. 3g,h,m,n**). In contrast, administration of water significantly increased c-Fos expression in *Ppp1r1b*[+] (**Fig. 3j,p**) but not in *Rspo2*^{+} neurons (**Fig. 3i,o**), compared to no water (**Fig. 3i,j,q,r**). The shock-specific activation of *Rspo2*^{+} aBLA cells and water-specific activation of *Ppp1r1b*^{+} pBLA cells were confirmed by further analyses of AP axis planes within aBLA and pBLA, respectively (**Supplementary Fig. 5**). However, these analyses also revealed some heterogeneity of

Figure 2 *Rspo2*^{+} and *Ppp1r1b*^{+} BLA neurons define spatially segregated populations of BLA pyramidal neurons. (**a**) Quantification of smFISH of *Rspo2* (green) and *Ppp1r1b* (red) expression across the AP axis (coronal distance from bregma –0.8 mm to –2.8 mm) of the BLA. Bars represent means; traces represent individual mice ($n = 3$). (**b**) Two sagittal views (ML distance from midline 3.2 mm, 3.4 mm) of double smFISH of *Rspo2* and *Ppp1r1b* with nuclear marker DAPI in the BLA (**c**) Coronal view of double smFISH of *Rspo2* and *Ppp1r1b* across the AP axis of the BLA. (**d–g**) Double smFISH of *Camk2a* and *Rspo2* (**d**), *Camk2a* and *Ppp1r1b* (**e**), *Gad1* and *Rspo2* (**f**) or *Gad1* and *Ppp1r1b* (**g**) in the BLA. Larger micrograph in **Supplementary Figure 3**. Scale bars: 500 µm (**b**), 200 µm (**c**), 25 µm (**d–g**). (**h**) Biocytin-filled magnocellular (top) and parvocellular (bottom) BLA neuron; scale bars, 50 µm. (**i**) Single-cell qPCR traces of *Rspo2* (green) and *Ppp1r1b* (red), from magnocellular (top) and parvocellular (bottom) BLA neurons. qPCR traces in which amplification occurred for either gene are shown; rfu, relative fluorescence units. (**j**) Electrophysiological response to current steps in a *Rspo2*^{+} (top) and *Ppp1r1b*[+] (bottom) BLA neuron. (**k**) Comparison of mean soma diameter (****$P < 0.0001$, $t(19) = 6.106$), membrane resistance (R_m; **$P = 0.0016$, $t(19) = 3.680$), and membrane capacitance (C_m; ****$P < 0.0001$, $t(19) = 4.734$) of qPCR-confirmed *Rspo2*^{+} (green, $n = 11$) and *Ppp1r1b*[+] (red, $n = 12$) neurons. Unpaired *t*-test. Results show mean ± s.e.m. (**a,k**).

Table 1 Genetic, anatomical, morphological and electrophysiological characterization of *Rspo2+* and *Ppp1r1b+* BLA neurons

	Rspo2+	*Ppp1r1b+*	*Rspo2+Ppp1r1b+*	
Total neurons ($n = 3$)	3,611	2,311	54	
Mean proportion (%)	59.9 ± 1.28	39.1 ± 1.14	0.970 ± 0.191	

	Rspo2+	*Gad1+*	*Rspo2+Gad1+*
Total neurons ($n = 1$)	303	112	0

	Ppp1r1b+	*Gad1+*	*Ppp1r1b+Gad1+*
Total neurons ($n = 1$)	190	116	0

	(Rspo2+Ppp1r1b)+Camk2+	*(Rspo2+Ppp1r1b)−Camk2+*	*(Rspo2+Ppp1r1b)+Camk2−*
Total neurons ($n = 4$)	2,361	0	0

	CTB-CeC+*Rspo2+*	CTB-CeC *Ppp1r1b+*
Total neurons ($n = 3$)	423	16
Mean proportion (%)	96.2 ± 0.945	3.78 ± 0.945

	CTB-CeL/CeM+*Rspo2+*	CTB-CeL/CeM+*Ppp1r1b+*
Total neurons ($n = 3$)	64	1,012
Mean proportion (%)	5.58 ± 1.74	94.4 ± 1.74

	CTB-NAc+*Rspo2+*	CTB-NAc+*Ppp1r1b+*
Total neurons ($n = 3$)	344	775
Mean proportion (%)	30.7 ± 3.53	69.2 ± 3.53

Cell type	Soma diameter (μm)	V_m (mV)	R_m (MΩ)	C_m (pF)	Spike threshold (mV)	Rheobase (pA)
Magnocellular ($n = 37$)	12.8 ± 0.2	−60.9 ± 0.9	103.1 ± 4.7	197.6 ± 10	−37.7 ± 0.4	213.7 ± 10.5
Parvocellular ($n = 38$)	9.4 ± 0.2	−55.6 ± 0.8	165.5 ± 6.5	102.2 ± 4.1	−35.5 ± 0.5	137.7 ± 6.7
Rspo2+ ($n = 10$)	13.1 ± 0.5	−62.5 ± 2.1	108.9 ± 9.6	190.3 ± 19.1	−37.6 ± 0.9	198.7 ± 18
Ppp1r1b+ ($n = 11$)	9.5 ± 0.3	−57.1 ± 1.5	158.7 ± 9.5	99.5 ± 5.9	−34.8 ± 1.1	152.3 ± 15.2

P-values	Soma diameter	V_m	R_m	C_m	Spike threshold	Rheobase
Magno- ($n = 37$) versus parvocellular ($n = 38$)	7×10^{-17}	0.00003	6×10^{-11}	1×10^{-11}	0.0008	8×10^{-8}
Rspo2+ ($n = 10$) versus *Ppp1r1b+* ($n = 11$)	0.00002	0.051	0.0016	0.0009	0.06	0.06
Magnocellular ($n = 27$) versus *Rspo2+* ($n = 10$)	0.5	0.4	0.5	0.7	0.9	0.4
Parvocellular ($n = 27$) versus *Ppp1r1b+* ($n = 11$)	0.6	0.3	0.5	0.6	0.5	0.2

Top, smFISH quantification of *Rspo2* and *Ppp1r1b* expression in the BLA, *Rspo2* and *Ppp1r1b* colocalization with *Gad1* in the BLA, combined probes for *Rspo2* and *Ppp1r1b* and their colocalization with *Camk2a* in the BLA, *Rspo2* and *Ppp1r1b* colocalization with CTB in CTB-injected mice (CeC, CeL/CeM, and NAc), cell counts corresponds to the total number of neurons counted in *n* animals. Bottom, *Rspo2+* and *Ppp1r1b+* BLA neurons correspond to magnocellular and parvocellular BLA neurons. Quantification of morphological (soma diameter) and electrophysiological properties (resting membrane potential (V_m), membrane resistance (R_m), capacitance (C_m), spike threshold, and rheobase) of all magnocellular and parvocellular neurons recorded and a subset of recorded neurons, which were qPCR-confirmed *Rspo2+* and *Ppp1r1b+* BLA neurons. *P*-values for unpaired *t*-test comparisons between all magnocellular and all parvocellular BLA neurons, qPCR-confirmed *Rspo2+* and *Ppp1r1b+* BLA neurons, qPCR-unconfirmed magnocellular and *Rspo2+* BLA neurons, qPCR-unconfirmed parvocellular and *Ppp1r1b+* BLA neurons; *n* corresponds to the number of neurons from at least 3 mice per group.

Rspo2+ neurons activated by shock within aBLA and *Ppp1r1b+* neurons activated by water within pBLA, relative to the neutral stimuli (**Supplementary Fig. 5**): *Rspo2+* neurons activated specifically by shock and *Ppp1r1b+* neurons activated specifically by water were distributed more posteriorly within aBLA and pBLA, respectively (**Supplementary Fig. 5**). Nevertheless, these data suggest that negative and positive information is represented by genetically defined populations of neurons in the BLA that are spatially segregated: *Rspo2+* neurons, which predominate in the aBLA, represent negative valence, while *Ppp1r1b+* neurons, which predominate in the pBLA, represent positive valence.

BLA in valence-specific behaviors

Valence-specific activation of *Rspo2+* and *Ppp1r1b+* neurons suggests that these populations may be necessary for valence-specific behaviors;

Figure 3 *Rspo2+* and *Ppp1r1b+* BLA neurons are activated by valence-specific stimuli. (**a**–**c**) c-Fos expression across the AP axis (coronal distance from bregma −0.8 mm to −2.8 mm) of the aBLA (top) and pBLA (bottom) in response to shock ($n = 8$), context ($n = 8$) or female ($n = 6$) (**a**); TMT ($n = 6$), benzaldehyde (BA) ($n = 7$) or peanut oil ($n = 6$) (**b**); and quinine water ($n = 8$), no water ($n = 8$), water ($n = 6$) or sucrose water ($n = 8$) (**c**). The total number of c-Fos+ cells is represented for each coronal section of a unilateral BLA; micrographs in **Supplementary Figure 4**. (**d**) Relative c-Fos expression in the aBLA and pBLA in response to shock, context or female (one-way ANOVA, $F_{2,19} = 33.91$, $P < 0.0001$). (**e**) Relative c-Fos expression in response to TMT, BA or peanut oil (one-way ANOVA, $F_{2,16} = 16.61$, $P = 0.0001$). (**f**) Relative c-Fos expression in response to quinine water, no water, water or sucrose water (one-way ANOVA, $F_{2,19} = 33.91$, $P < 0.0001$). Significance for multiple comparisons (**d**–**f**), *$P < 0.05$, **$P < 0.01$, ****$P < 0.0001$; N.S., not significant. Shock vs. female, $P < 0.0001$; shock vs. context, $P = 0.0010$; context vs. female, $P = 0.0013$; TMT vs. BA, $P = 0.0377$; TMT vs. peanut, $P < 0.0001$; BA vs. peanut, $P = 0.0132$; water vs. quinine, $P < 0.0001$; water vs. sucrose, $P = .9998$; water vs. no water, $P < 0.0001$; quinine vs. sucrose, $P < 0.0001$; quinine vs. no water, $P = 0.3500$; sucrose vs. no water, $P < 0.0001$. (**g**–**r**) Double-label smFISH ($n = 5$ in each group) of *Fos+Rspo2+* (**g,k,m**) or *Fos+Ppp1r1b+* (**h,l,n**) in response to shock (S) or context (C). Double-label smFISH of *Fos* and *Rspo2* (**i,o,q**) or of *Fos* and *Ppp1r1b* (**j,p,r**) in response to water (W) or no water (NW) (AP axis analysis in **Supplementary Fig. 5**); *y*-axis values denote percentage of double-positive cells. Significance for unpaired *t*-test (**g**–**j**), **$P < 0.01$; N.S., not significant; (**g**) $P = 0.0098$, $t(8) = 3.371$; (**h**) $P = 0.2222$, $t(10) = 1.302$; (**i**) $P = 0.5685$, $t(8) = 0.5946$; (**j**) $P = 0.0013$, $t(8) = 4.822$. Scale bars, 125 μm (**k**–**r**). Results show mean ± s.e.m. (**a**–**j**). Colors: valence of the stimuli negative (green) and positive (red) in **a**–**j**; *Rspo2* (green) and *Ppp1r1b* (red) in **k**–**r**.

therefore, we studied the effects of inhibiting these BLA populations in fear and reward conditioning experiments. $Rspo2^+$ and $Ppp1r1b^+$ neurons were genetically targeted using Rspo2-Cre and Cartpt-Cre mice, respectively. $Ppp1r1b^+$ BLA neurons are genetically accessible through cocaine- and amphetamine-regulated transcript protein (Cartpt) Cre driver mice (Cartpt-Cre) (**Supplementary Fig. 6**), and hereafter, virus-injected Cartpt-Cre mice will be referred to using "Ppp1r1b." The light-activated inhibitory ion channel eArch3.0 was

expressed in $Rspo2^+$ (Rspo2-Arch) and $Ppp1r1b^+$ (Ppp1r1b-Arch) BLA neurons using a Cre-dependent viral vector (AAV$_5$-EF1α-DIO-eArch3.0-eYFP) bilaterally targeted to the BLA of Rspo2-Cre and Cartpt-Cre mice, respectively. Control mice (Rspo2-eYFP, Ppp1r1b-eYFP) received a viral vector lacking eArch3.0 (AAV$_5$-EF1α-DIO-eYFP) (**Fig. 4a,l,m** and **Supplementary Fig. 7**).
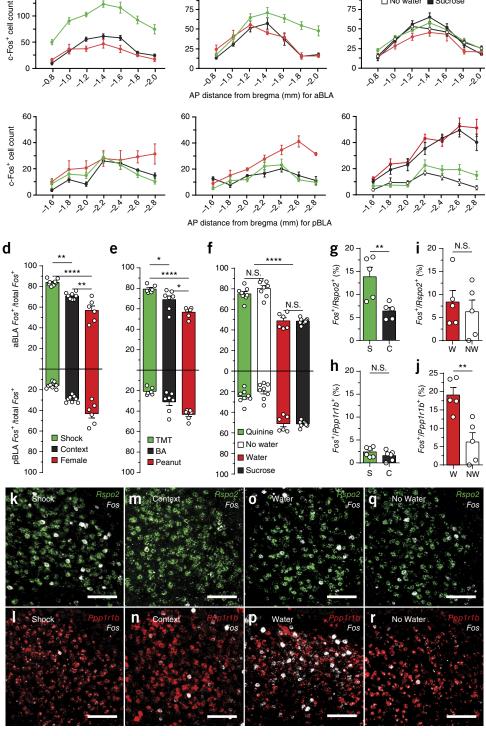
On day 1 of contextual fear conditioning, mice received green light, bilaterally targeted to the BLA during footshocks (**Fig. 4b**). Rspo2-Arch

mice displayed reduced levels of freezing in response to footshocks compared with Rspo2-eYFP mice. Ppp1r1b-Arch mice displayed similar levels of freezing compared to Ppp1r1b-eYFP mice. On day 2, mice were tested in the context without shock or light stimulation. Less freezing was observed in Rspo2-Arch mice than in Rspo2-GFP mice, while similar levels of freezing were observed in Ppp1r1b-Arch mice compared to Ppp1r1b-eYFP mice (**Fig. 4c**). Thus, Rspo2^{+}, but not Ppp1r1bp[+], BLA neuronal activity is critical for freezing to shock stimuli and for the association of a context to freezing behavior.

Reward conditioning took place in an operant conditioning chamber where water was dispensed contingent on a nose poke following an external light cue (**Fig. 4d**). Green light was bilaterally delivered into the BLA simultaneously with the presentation of water. Rspo2-Arch and Rspo2-eYFP mice displayed similar levels of nose pokes and cue–reward association (z-score of time spent in the reward port during cue period; see Online Methods). In contrast, Ppp1r1b-Arch mice displayed reduced levels of nose pokes and cue–reward association compared to Ppp1r1b-eYFP mice (**Fig. 4e**). Thus, *Ppp1r1b*[+], but not *Rspo2*^{+}, BLA neuronal activity is critical for reward-seeking behavior and for the association of a conditioned stimulus to appetitive behavior.

Next we assessed the effects of activating these BLA neurons. The light-activated excitatory ion channel ChR2 was expressed in *Rspo2*^{+} (Rspo2-ChR2) and *Ppp1r1b*[+] (Ppp1r1b-ChR2) BLA neurons using a Cre-dependent viral vector (AAV_5-EF1α-DIO-ChR2-eYFP) unilaterally targeted to the BLA of Rspo2-Cre and Cartpt-Cre mice, respectively. Control mice (Rspo2-eYFP, Ppp1r1b-eYFP) received a viral vector lacking ChR2 (AAV_5-EF1α-DIO-eYFP) (**Fig. 4a,n,o**).

On day 1 of the optogenetic freezing test, mice were placed in a neutral context while receiving blue light stimulation (**Fig. 4f** and Online Methods). Rspo2-ChR2 mice displayed greater levels of freezing compared to Rspo2-eYFP mice, while Ppp1r1rb-ChR2 and Ppp1r1b-eYFP mice displayed similar levels of freezing (**Fig. 4g**). On day 2, mice were returned to the context and freezing was measured without shock. Rspo2-ChR2 mice displayed greater levels of freezing than Rspo2-eYFP mice, while Ppp1r1rb-ChR2 and Ppp1r1b-eYFP mice displayed similar levels of freezing (**Fig. 4g**). Thus, *Rspo2*^{+}, but not *Ppp1r1b*[+], BLA neurons are capable of eliciting freezing, which can be conditioned to a neutral context.

On day 1 of the optogenetic self-stimulation test, mice were placed in an operant conditioning chamber in which blue light stimulation was administered when the mouse poked into a nose port (**Fig. 4h**). Ppp1r1b-ChR2 mice made a greater number of pokes than Ppp1r1b-eYFP mice, while Rspo2-ChR2 and Rspo2-eYFP mice made similar

numbers of pokes. On day 2, mice were returned to the operant condition chamber, in which no light stimulation was delivered. Ppp1r1b-ChR2 mice made more pokes than Ppp1r1b-eYFP mice, while Rspo2-ChR2 and Rspo2-eYFP mice made similar numbers of pokes (**Fig. 4i**). Thus, *Ppp1r1b*[+], but not *Rspo2*^{+}, BLA neurons are capable of eliciting self-stimulation and support reward conditioning.

In a real-time optogenetic place preference test (**Fig. 4j**), Rspo2-ChR2 mice spent less time in the light-stimulated side compared to corresponding controls, while Ppp1r1b-ChR2 mice spent more time in the light-stimulated side compared to corresponding controls (**Fig. 4k**). Therefore, *Rspo2*^{+} BLA neurons are capable of eliciting place aversion while *Ppp1r1b*^{+} BLA neurons are capable of eliciting place preference.

Antagonism between negative and positive BLA neurons

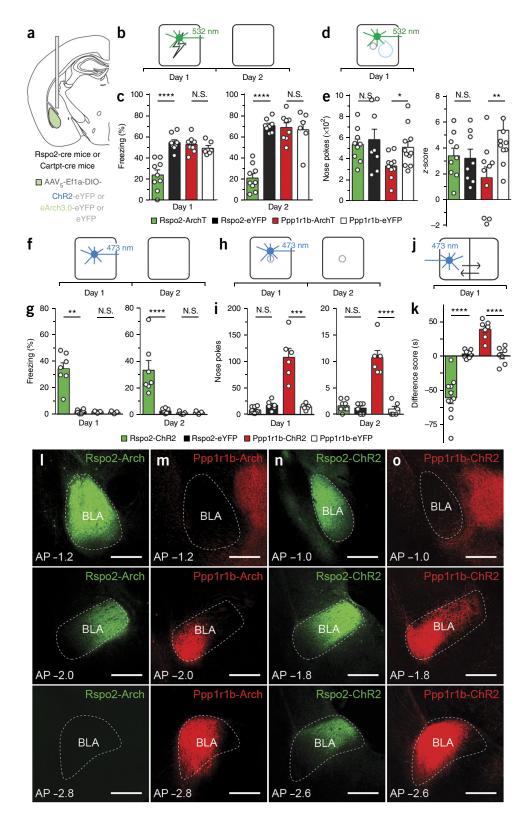*Rspo2*^{+} and *Ppp1r1b*^{+} neurons drive opposing behaviors; therefore, we examined whether these two types of neurons contribute to the antagonistic control of emotional behaviors and memories. For this purpose, we examined the behavioral effects of optogenetically activating *Rspo2*^{+} or *Ppp1r1b*^{+} neurons during the presence of valence-specific stimuli. On day 1 of contextual fear conditioning, ChR2-expressing mice received bilateral blue light stimulation in the BLA during footshocks (**Fig. 5a**). Rspo2-ChR2 and Rspo2-eYFP mice displayed similar levels of freezing in response to footshocks, while Ppp1r1b-ChR2 mice displayed lower levels of freezing than Ppp1r1b-eYFP mice (**Fig. 5b,c**). On day 2, conditioned freezing was assessed by returning mice to the context without footshock or light stimulation. As on day 1, no difference in freezing was observed between Rspo2-ChR2 and Rspo2-eYFP mice, while less freezing was observed in Ppp1r1b-ChR2 mice than in Ppp1r1b-eYFP mice (**Fig. 5b,c**). Thus, activation of *Ppp1r1b*^{+} BLA neurons is capable of disrupting freezing to footshocks and the association of a conditioned contextual stimulus with footshocks.

In reward conditioning, ChR2-expressing mice received blue light stimulation during reward delivery (**Fig. 5d**). Rspo2-ChR2 displayed reduced levels of nose pokes and cue–reward association compared to Rspo2-eYFP mice, while Ppp1r1b-ChR2 and Ppp1r1bp-eYFP mice displayed similar levels of nose pokes and cue–reward association (**Fig. 5e,f**). Thus, activation of *Rspo2*^{+} BLA neurons is capable of disrupting reward-seeking behaviors and the association of a conditioned stimulus with a reward.

Although *Rspo2*^{+} and *Ppp1r1b*^{+} neurons antagonize behaviors elicited by stimuli of the opposing valence, behavioral antagonism may be result of interference by downstream circuits rather than by direct interactions between these two neuronal populations. Therefore, the

Figure 4 *Rspo2*^{+} and *Ppp1r1b*^{+} BLA neurons participate in valence-specific behaviors. (**a**) Optogenetically targeting *Rspo2*^{+} and *Ppp1r1b*^{+} BLA neurons. (**b–e**) Scheme and results for Rspo2-Arch and Ppp1r1b-Arch mice in fear (**b,c**) and reward (**d,e**) conditioning. (**c**) Rspo2-Arch mice ($n = 9$) froze less on days 1 and 2 than eYFP controls ($n = 8$); no difference between Ppp1r1b-Arch ($n = 8$) and Ppp1r1b-eYFP ($n = 6$) mice. Rspo2, day 1 $P < 0.0001$, $t(15) = 5.366$, day 2 $P < 0.0001$, $t(15) = 10.24$; Ppp1r1b, day 1 $P = 0.3700$, $t(12) = 0.9314$, day 2 $P = 0.8268$, $t(12) = 0.2237$. (**e**) Ppp1r1b-Arch mice ($n = 10$) displayed lower total nose pokes and cue–reward association in nose port (z-score) compared to eYFP controls ($n = 11$); no difference between Rspo2-Arch ($n = 9$) and Rspo2-eYFP ($n = 8$). Rspo2, pokes $P = 0.6811$, $t(15) = 0.4191$, z-score $P = 0.8510$, $t(15) = 0.1911$; Ppp1r1b, pokes $P = 0.0192$, $t(19) = 2.55$, z-score $P = 0.0097$, $t(19) = 2.873$. (**f–k**) Scheme and results for Rspo2-ChR2 and Ppp1r1b-ChR2 mice in an optogenetic freezing test (**f,g**), optogenetic self-stimulation test (**h,i**), and optogenetic place preference test (**j,k**). (**g**) Rspo2-ChR2 mice ($n = 7$) froze more on days 1 and 2 than eYFP controls ($n = 6$); no difference between Ppp1r1b-ChR2 ($n = 5$) and Ppp1r1b-eYFP ($n = 5$) mice. Rspo2, day 1 $P = 0.0020$, $t(12) = 3.926$, day 2 $P < 0.0001$, $t(12) = 6.216$; Ppp1r1b, day 1 $P = 0.5408$, $t(8) = 0.6388$, day 2 $P = 0.4784$, $t(8) = 0.7435$. (**i**) Ppp1r1b-ChR2 mice ($n = 6$) made more nose pokes on days 1 and 2 than eYFP controls ($n = 6$); no difference between Rspo2-ChR2 ($n = 8$) and Rspo2-eYFP ($n = 6$) mice. Rspo2, day 1 $P = 0.0528$, $t(12) = 2.148$, day 2 $P = 0.4256$, $t(12) = 0.8247$; Ppp1r1b, day 1 $P = 0.0003$, $t(10) = 5.479$, day 2 $P < 0.0001$, $t(10) = 6.550$. (**k**) Rspo2-ChR2 mice ($n = 11$) displayed greater preference for light stimulation than eYFP controls ($n = 8$); Ppp1r1b-ChR2 ($n = 7$) mice displayed greater preference for light stimulation than eYFP controls ($n = 7$). Rspo2, $P < 0.0001$, $t(17) = 5.969$; Ppp1r1b, $P = 0.0001$, $t(12) = 5.589$. Significance for unpaired t-test between experimental groups compared to corresponding eYFP controls, *$P < 0.05$, **$P < 0.01$, ***$P < 0 0.001$, ****$P < 0.0001$; N.S., not significant; results show mean ± s.e.m. (**c,e,g,i,k**). (**l–o**) Expression of eArch-eYFP in Rspo2-Arch mice (**l**) and Ppp1r1b-Arch mice (**m**). Expression of ChR2-eYFPin Rspo2-ChR2 mice (**n**) and Ppp1r1b-ChR2 mice (**o**). Strong Ppp1r1b[+] fibers are found in the central amygdala (**m,o**). Scale bars, 300 µm (**l–o**). Colors: Rspo2-Cre mice (green) and Cartpt-Cre mice (red) (**c,e,g,i,k,l–o**).

effect of optogenetic activation of one of the two neuronal populations on the activation of the other in response to valence-specific stimuli was measured using *Fos*. In Ppp1r1b-ChR2 mice, which received blue light stimulation in the presence of footshocks, *Fos* was increased in *Ppp1r1b*^{+} neurons and decreased in *Rspo2*^{+} neurons compared to Ppp1r1b-eYFP mice (**Fig. 5g,h,i**). In water-deprived Rspo2-ChR2

mice, which received blue light stimulation during the consumption of water, *Fos* was increased in *Rspo2*^{+} neurons and decreased in *Ppp1r1b*^{+} neurons compared to that in Rspo2-eYFP mice (**Fig. 5j,k,l**). Thus, *Ppp1r1b*[+] and *Rspo2*^{+} neurons are capable of reducing the activity elicited by valence-specific stimuli in the opposite neuronal population.
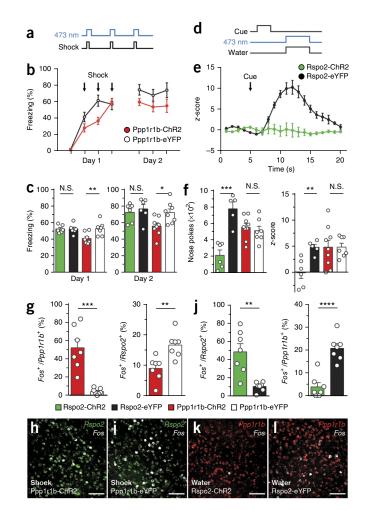
Figure 5 *Rspo2*^{+} and *Ppp1r1b*^{+} BLA neurons antagonize valence-specific behaviors. (**a**) Scheme of activation of BLA neurons in Rspo2-ChR2 and Ppp1r1b-ChR2 mice during shocks (day 1). (**b**) Time course of freezing during day 1 and day 2 in Ppp1r1b-ChR2 (*n* = 8) and Ppp1r1b-eYFP (*n* = 8) mice. (**c**) On day 1 and day 2, Ppp1r1b-ChR2 (*n* = 8) froze less than eYFP controls (*n* = 8), no difference between Rspo2-ChR2 (*n* = 6) and Rspo2-eYFP (*n* = 6) mice. *Rspo2*, day 1 *P* = 0.9684, *t*(10) = 0.04056, day 2 *P* = 0.5777, *t*(10) = 0.5755; *Ppp1r1b*, day 1 *P* = 0.0055, *t*(14) = 3.275, day 2 *P* = 0.0171, *t*(14) = 2.705. (**d**) Scheme of activation of BLA neurons in Rspo2-ChR2 and Ppp1r1b-ChR2 mice during reward conditioning. (**e**) Time course of *z*-score of poking in Rspo2-ChR2 (*n* = 6) and Rspo2-eYFP (*n* = 5) mice. (**f**) Rspo2-ChR2 mice (*n* = 6) displayed lower total nose pokes and cue–reward association compared to eYFP controls (*n* = 5), no difference between Ppp1r1b-ChR2 (*n* = 9) and Ppp1r1b-eYFP (*n* = 7) mice. Unpaired *t*-test between experimental groups and corresponding eYFP controls. *Rspo2*: pokes *P* = 0.0003, *t*(9) = 5.604; *z*-score *P* = 0.0002, *t*(9) = 6.209; *Ppp1r1b*: pokes *P* = 0.5990, *t*(14) = 0.5381; *z*-score *P* = 0.9986, *t*(14) = 0.001757. (**g**–**i**) Quantification of smFISH of *Fos* in *Ppp1r1b*[+]and *Rspo2*^{+} neurons in Ppp1r1b-ChR2 and Ppp1r1b-eYFP mice that received shock simultaneously with blue light stimulation. (**j**–**l**) Quantification of smFISH of *Fos* in *Rspo2*^{+} and *Ppp1r1b*^{+} neurons in Rspo2-ChR2 and Rspo2-eYFP mice that received water simultaneously with blue light stimulation. Unpaired *t*-test (**g**,**j**). (**g**) Left *P* = 0.0002, *t*(12) = 5.377; right *P* = 0.0035, *t*(12) = 3.616. (**j**) Left *P* = 0.0013, *t*(12) = 4.180; right *P* < 0.0001, *t*(12) = 6.012. Scale bars, 300 μm (**h**,**i**,**k**,**l**). Colors: Rspo2-Cre mice (green) and Cartpt-Cre mice (red) (**b**,**c**,**e**–**g**,**j**) or valence of stimuli negative (green) and positive (red or white) (**h**,**i**,**k**,**l**). Results show mean ± s.e.m. (**b**,**c**,**e**,**f**,**g**,**j**). **P* < 0.05, **P < 0.01, ***P < 0 0.001, ****P < 0.0001; N.S., not significant.

Antagonism of valence-specific BLA neurons observed at the behavioral and *Fos* activation level was further examined at the microcircuit level by combining patch clamp recording with optogenetic stimulation of valence-specific neurons. The functional relationship between *Rspo2*^{+} and *Ppp1r1b*^{+} neurons were examined by combining patch clamp recordings with optogenetic stimulation of cell-type-specific axons (**Fig. 6a–d**). Patch clamp recordings of *Rspo2*^{+} and *Ppp1r1b*^{+} neurons revealed distinct intrinsic physiological properties (**Table 1**). Therefore, the postsynaptic cell target was recognized on the basis of a combination of anatomical position, soma size, and intrinsic electrophysiological properties (**Fig. 6m,n**). Electrophysiological recordings of *Rspo2*^{+} neurons in response to optogenetic stimulation of Ppp1r1b-ChR2^{+} fibers and recordings of *Ppp1r1b*^{+} neurons in response to stimulation of Rspo2-ChR2^{+} fibers showed inhibitory postsynaptic potentials (**Fig. 6e–h,k,l**). The probability of connections of *Rspo2*^{+} to *Ppp1r1b*[+]and vice versa were 100% and 100% inhibitory, respectively (**Fig. 6i,j**), of which 25% of connections of *Ppp1r1b*[+] to *Rspo2*^{+}BLA neurons and 17% of connections of *Rspo2*^{+}to *Ppp1r1b*[+]were both inhibitory and excitatory (**Fig. 6i,j**). These data suggest that these two populations interact predominantly through mutual inhibition.

Projections from negative and positive BLA neurons

The distinct projection targets of the *Rspo2*^{+} and *Ppp1r1b*^{+} neurons may reveal divergent brain structures that mediate negative and positive behaviors. Therefore, retrograde tracing from putative projection targets was examined using cholera toxin subunit b (CTB). CTB targeted to the capsular nucleus of the central amygdala (CeC) labeled neurons primarily in the aBLA (**Fig. 7a,c,d**). CTB targeted to the lateral and medial nucleus of the central amygdala (CeL/CeM) labeled neurons distributed along the lateral side of the pBLA (**Fig. 7a,e,f**). CTB targeted to the nucleus accumbens (NAc) labeled neurons distributed along the medial side of the BLA, spanning the posterior end of the aBLA to the posterior end of the pBLA (**Fig. 7a,g,h**). Dual-labeled CTB targeted to the prelimbic (PL) and infralimbic (IL) cortex labeled spatially segregated distributions of neurons in the BLA—PL-CTB^{+} neurons primarily in the aBLA, IL-CTB^{+} neurons primarily in the pBLA (**Fig. 7b,i,j**). smFISH with *Rspo2* or *Ppp1r1b* probe in CTB-injected mice revealed that CeC-CTB^{+} BLA neurons were 96% *Rspo2*^{+} and 4% *Ppp1r1b*[+]; CeL/CeM-CTB^{+} neurons were 6% *Rspo2*^{+} and 94% *Ppp1r1b*[+]; NAc CTB^{+} neurons were 30% *Rspo2*^{+} and 70% *Ppp1r1b*[+] (**Fig. 7k–n**, **Table 1** and **Supplementary Fig. 8**).

For anterograde characterization, we examined ChR2-eYFP[+] fibers in Rspo2-ChR2 and Ppp1r1b-ChR2 mice. In Rspo2-ChR2 mice, dense fibers were found in the CeC, NAc, and PL, but not in the CeL, CeM, or IL (**Fig. 7o**). In Ppp1r1b-ChR2 mice, dense fibers were found in the CeL, CeM, NAc and IL but not in the CeC or PL (**Fig. 7p**). Together, CTB retrograde tracing and anterograde characterization of projection fibers suggest that *Rspo2*^{+} distinctly project to the CeC and PL, *Ppp1r1b*^{+} neurons distinctly project to the CeL, CeM, and IL, and both *Rspo2*^{+} and *Ppp1r1b*^{+} BLA neurons both project to the NAc.

DISCUSSION

Here we employed a forward genetic strategy to transcriptionally profile active neurons in BLA. This approach revealed genetic markers for distinct populations of BLA neurons and predicted neuronal function. *Rspo2*^{+} BLA neurons are activated by stimuli that elicit negative behaviors, while *Ppp1r1b*^{+} BLA neurons are activated by stimuli that elicit positive behaviors. *Rspo2*^{+} BLA neurons are crucial for negative behaviors and associations, while *Ppp1r1b*^{+} BLA neurons are crucial for positive behaviors and associations. *Rspo2*^{+} and *Ppp1r1b*^{+} neurons are antagonistic at the behavioral, neuronal
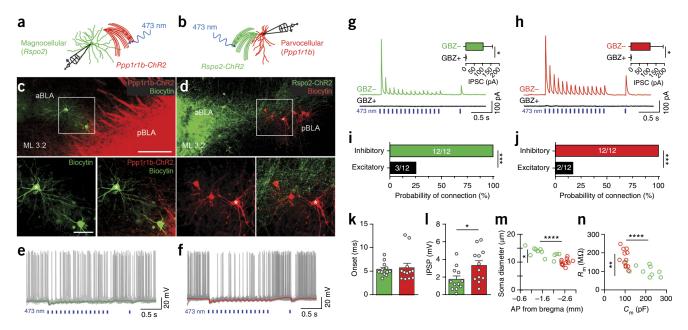
Figure 6 *Rspo2*^{+} and *Ppp1r1b*^{+} BLA neurons establish reciprocal inhibitory connections. (**a,b**) Scheme for the experimental setup for recording in magnocellular (*Rspo2*^{+}) (**a**) and parvocellular (*Ppp1r1b*[+]) (**b**) neurons, while stimulating *Ppp1r1b*[+] (Ppp1r1b-ChR2 mice) and *Rspo2*^{+} (Rspo2-ChR2 mice) neurons, respectively. (**c,d**) Sagittal view of biocytin-filled *Rspo2*^{+} BLA neurons in Ppp1r1b-ChR2 mice (**c**) and *Ppp1r1b*^{+} BLA neurons in Rspo2-ChR2 mice (**d**). Main scale bar, 200 μm; inset, 50 μm. Asterisks in **c** and **d** denote the cells recorded in **e** and **f**, respectively. (**e,f**) Inhibitory postsynaptic potentials recorded in *Rspo2*^{+} (**e**) and *Ppp1r1b*[+] (**f**) BLA neurons by 10-Hz optogenetic stimulation of Ppp1r1b-ChR2 (**e**) and Rspo2-ChR2 (**f**) fibers. Green (**e**) and red (**f**) traces represent average trace of 20 sweeps recorded during periods without spikes. (**g,h**) Inhibitory postsynaptic currents (IPSCs) recorded in *Rspo2*^{+} (magnocellular; **g**) and *Ppp1r1b*[+] (parvocellular; **h**) BLA neurons (clamped at 0 mV) in response to optogenetic stimulation (10-Hz train) of Ppp1r1b-ChR2 (**g**) and Rspo2-ChR2 (**h**) fibers. Currents are blocked by bath application of gabazine (GBZ, 10 μM); insets: IPSC amplitude before (GBZ−) and after (GBZ+) GBZ application (for both magnocellular ($n = 6$) (**g**) and parvocellular ($n = 6$) (**h**) neurons, Wilcoxon signed-rank test, *$P = 0.0313$. (**i,j**) Probability of connection, *Ppp1r1b*[+] to *Rspo2*^{+} connection (**i**) and *Rspo2*^{+} to *Ppp1r1b*[+] connection (**j**). The two groups interact predominately by mutual inhibition rather than excitation; Fisher exact test, ***$P < 0.001$. (**k**) IPSC onset in *Rspo2*^{+} (green) and *Ppp1r1b*[+] (red) neurons were similar. (**l**) IPSC amplitude was greater in *Ppp1r1b*[+] (red) than in *Rspo2*^{+} (green) neurons; unpaired *t*-test, *$P < 0.05$. (**m,n**) Recorded magnocellular (green) and parvocellular (red) neurons were confirmed using soma diameter and anatomical position (**m**) and membrane resistance (R_m) and membrane capacitance (C_m) (**n**). *Rspo2*^{+} and *Ppp1r1b*^{+} cells were statistically distinct in all four parameters and consistent with values characterized in **Figure 2**; unpaired *t*-test *$P < 0.05$, **$P < 0.01$, ****$P < 0.0001$ (**m,n**). (**k**) $P = 0.7441$, $t(22) = 0.3305$; (**l**) $P = 0.0216$, $t(22) = 2.472$; (**m**) AP distance from bregma $P < 0.0001$, $t(22) = 6.681$; soma $P < 0.0001$, $t(22) = 5.857$; (**n**) C_m $P < 0.0001$, $t(22) = 5.677$, R_m $P = 0.0003$, $t(22) = 4.341$. Results show mean ± s.e.m. (**g,h,k,l**). Colors: neurons recorded or virus-infected transgenic mouse, *Rspo2*^{+} neurons or Rspo2-Cre (green) and *Ppp1r1b*^{+} neurons or Cartpt-Cre (red) (**a–n**).

population, and electrophysiological levels. They not only drive opposing behaviors, but also antagonize valence-specific behaviors, antagonize the overall activation of the opposing neurons and interact through reciprocal feedforward inhibition. Collectively, these results support a model in which mutually inhibitory *Rspo2*^{+} and *Ppp1r1b*^{+} neurons are the principal neurons that represent and elicit negative and positive behaviors, respectively.

Previous inactivation studies have implicated a greater contribution of the aBLA in contextual fear conditioning[12] and the pBLA in reward conditioning[27]. Here we dissociated, using specific genetic markers for cell-type-specific manipulations, the participation of the aBLA and pBLA in negative and positive behaviors, respectively. Although *Rspo2*^{+} and *Ppp1r1b*^{+} neurons constitute virtually all BLA pyramidal neurons, there may be further functional, genetic, and or structural diversity within each of these two cell types. Other genetic markers found as candidates on our screen were not pursued in this study, but further studies could be performed to examine the role of other genetically distinct BLA neurons, and these studies may reveal functionally distinct subsets of neurons within *Rspo2*^{+} negative neurons or within *Ppp1r1b*^{+} positive neurons. However, from the examination of *Rspo2*^{+} and *Ppp1r1b*^{+} neurons in a set of behavioral assays (**Fig. 4**), we found no evidence suggesting that *Rspo2*^{+} and

Ppp1r1b^{+} neurons participate in behaviors or associations across valence. Together, these findings add to the growing evidence of the spatially segregated representation of negative and positive information in the brain, as demonstrated in the medial amygdala[28], cortical amygdala[29] and gustatory cortex[30] in mice, and dopaminergic and mushroom body neurons in *Drosophila*[31,32]. Thus, spatially segregated representation of negative and positive information may be a common motif throughout the CNS and across invertebrate and vertebrate species.

Previous *in vivo* electrophysiology and stimulus-dependent studies suggested that negative and positive BLA neurons may be intermingled[15,16]. However, our results suggest that negative and positive neurons are spatially segregated into the aBLA and pBLA, respectively. At the transition between the aBLA and pBLA, these two types of neurons can be considered intermingled; however, examination of the entire BLA showed that *Rspo2* and *Ppp1r1b* are spatially segregated in the BLA and define what has previously been defined as the anterior and posterior subfields of the BLA and correspond to magnocellular and parvocellular neurons, respectively[4].
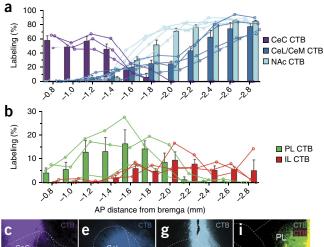
The identification of a mutually inhibitory microcircuit between negative and positive neurons suggests that the BLA is a key site for the antagonistic control of affective emotional states and emotional
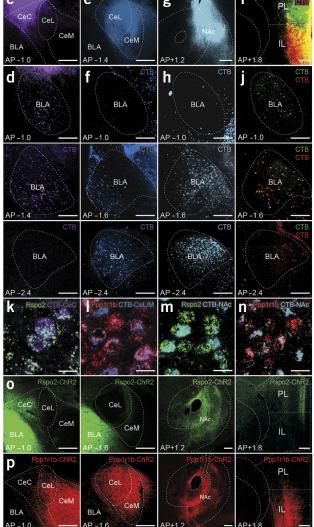
Figure 7 *Rspo2*^{+} and *Ppp1r1b*^{+} BLA neurons project to distinct amygdaloid nuclei and prefrontal areas. (**a**–**j**) Quantification of CTB^{+} neurons across the AP axis (coronal distance from bregma −0.8 mm to −2.8 mm) of the BLA from CTB targeted to the amygdala and supplemental amygdala areas (**a**)—CeC (**c**,**d**), CeL/CeM (**e**,**f**), NAc (**g**,**h**)—or dual CTB targeted to prefrontal cortex (**b**)—PL and IL (**i**,**j**) (bars represent mean, traces represent individual mice, *n* = 3 mice per group). Injections site of CTB (**c**,**e**,**g**,**i**) and CTB^{+} BLA neurons (**d**,**f**,**h**,**j**). (**k**,**m**) Colabeling of *Rspo2* mRNA in the BLA with CTB targeted to the CeC (**k**) and NAc (**m**). (**l**,**n**) Co-labeling of *Ppp1r1b* mRNA in the BLA with CTB injected into the CeL/CeM (**l**) and NAc (**n**); quantification in **Table 1**, micrographs in **Supplementary Figure 7**. (**o**) Rspo2-ChR2^{+} fibers are found in the CeC, NAc, and PL. (**p**) Ppp1r1b-ChR2^{+} fibers are found in the CeL, CeM, NAc, and IL. Colors: Rspo2-Cre mice (green) and Cartpt-Cre mice (red) (**o**,**p**). Scale bars: 250 μm (**c**–**j**,**o**,**p**), 25 μm (**k**–**n**). Results show mean ± s.e.m.

memories. The antagonistic BLA circuit provides a circuit mechanism for representing and associating a continuous range of negative and positive information on the basis of the balance of excitation between these two populations. Studies have correlated negative affective states with elevated excitability in the BLA[33,34], which suggest that the imbalance of excitation between negative and positive BLA neurons may be an underlying mechanism in emotional disorders. Therefore, the identification of distinct molecular markers for neurons that participate in an antagonistic circuit provides an avenue for more precise cellular and pharmacological targeting for the treatment of disease, in addition to genetic models for further elucidation of the circuitry and mechanisms underlying emotional behavior and memories.

Previous studies have targeted BLA neurons for the study of negative and positive behaviors using projection target-based criteria[18]. These studies suggested that NAc projections may be a defining feature of positive BLA neurons[18]. However, retrograde and antero-grade projection experiments showed that ~30% of BLA neurons that projected to NAc were *Rspo2*^{+} BLA neurons. Furthermore, stimulation of *Rspo2*^{+} somata or their NAc projections resulted in negative behaviors (**Supplementary Fig. 9**). These findings demonstrate that such a projection-based definition is insufficient for distinguishing negative and positive BLA neurons[34]. Previous observations that BLA-to-NAc projections mediate positive behaviors[8,16] are likely due to the observation that a larger proportion of NAc-projecting BLA neurons are *Ppp1r1b*[+] (**Table 1**).

It is widely thought that the amygdala fear circuit involves direct transmission of negative information from BLA principal neurons to CeL neurons and/or effector neurons in the CeM[18,35–38]. Contrary to these previous hypotheses, our data suggest that positive but not negative BLA neurons project to the CeM and CeL, while negative but not positive BLA neurons project to the CeC. Here, the previous projection-based definition of BLA neurons—namely, that the neurons projecting directly to the CeM drive negative behavior[18,35–38]—is not supported by our findings. In regards to CeM and CeL projections, our findings are consistent with anatomical studies demonstrating that parvocellular BLA neurons (which are *Ppp1r1b*[+]) send strong projections to the CeL and CeM and provide further support for the role of the central amygdala in appetitive behaviors[26,39–43]. In regards to connections from negative BLA neurons to effector neurons in the CeM, our findings suggest that this may be an indirect route through the CeC. A recent study identified a population of *Calcrl*^{+} neurons in the CeC and CeL, which supports negative behaviors similarly to *Rspo2*^{+} BLA neurons and thus may be an intermediate between negative BLA neurons and the putative CeM effector neurons[44]. Overall, the identification of genetic markers for distinct populations of BLA neurons has permitted the functional and anatomical dissociation

of the circuit underlying negative and positive behaviors, in turn, providing a revised functional and structural model of the BLA (**Supplementary Fig. 10**).

METHODS

Methods, including statements of data availability and any associated accession codes and references, are available in the online version of the paper.

AUTHOR CONTRIBUTIONS

J.K. and S.T. conceived the study. J.K. identified gene markers. S.I. generated the transgenic Rspo2-Cre mouse. J.K. collected and analyzed histological data. J.K. and S.X., collected and analyzed behavioral data. M.P. collected and analyzed electrophysiological data. J.K. and S.T. wrote the manuscript. J.K., M.P., S.X., S.I. and S.T. discussed and commented on the manuscript.

COMPETING FINANCIAL INTERESTS

The authors declare no competing financial interests.

Reprints and permissions information is available online at http://www.nature.com/reprints/index.html.

1. Pitkänen, A., Savander, V. & LeDoux, J.E. Organization of intra-amygdaloid circuitries in the rat: an emerging framework for understanding functions of the amygdala. *Trends Neurosci.* **20**, 517–523 (1997).
2. McDonald, A.J. Neuronal organization of the lateral and basolateral amygdaloid nuclei in the rat. *J. Comp. Neurol.* **222**, 589–606 (1984).
3. Swanson, L.W. & Petrovich, G.D. What is the amygdala? *Trends Neurosci.* **21**, 323–331 (1998).
4. Hall, E. The amygdala of the cat: a Golgi study. *Z. Zellforsch. Mikrosk. Anat.* **134**, 439–458 (1972).
5. McDonald, A.J. Neurons of the lateral and basolateral amygdaloid nuclei: a Golgi study in the rat. *J. Comp. Neurol.* **212**, 293–312 (1982).
6. Carlsen, J. & Heimer, L. The basolateral amygdaloid complex as a cortical-like structure. *Brain Res.* **441**, 377–380 (1988).
7. Mascagni, F. & McDonald, A.J. A novel subpopulation of 5-HT type 3A receptor subunit immunoreactive interneurons in the rat basolateral amygdala. *Neuroscience* **144**, 1015–1024 (2007).
8. McDonald, A.J., Muller, J.F. & Mascagni, F. GABAergic innervation of alpha type II calcium/calmodulin-dependent protein kinase immunoreactive pyramidal neurons in the rat basolateral amygdala. *J. Comp. Neurol.* **446**, 199–218 (2002).
9. Redondo, R.L. *et al.* Bidirectional switch of the valence associated with a hippocampal contextual memory engram. *Nature* **513**, 426–430 (2014).
10. Stuber, G.D. *et al.* Excitatory transmission from the amygdala to nucleus accumbens facilitates reward seeking. *Nature* **475**, 377–380 (2011).
11. Ambroggi, F., Ishikawa, A., Fields, H.L. & Nicola, S.M. Basolateral amygdala neurons facilitate reward-seeking behavior by exciting nucleus accumbens neurons. *Neuron* **59**, 648–661 (2008).
12. Goosens, K.A. & Maren, S. Contextual and auditory fear conditioning are mediated by the lateral, basal, and central amygdaloid nuclei in rats. *Learn. Mem.* **8**, 148–158 (2001).
13. Cador, M., Robbins, T.W. & Everitt, B.J. Involvement of the amygdala in stimulus-reward associations: interaction with the ventral striatum. *Neuroscience* **30**, 77–86 (1989).
14. Killcross, S., Robbins, T.W. & Everitt, B.J. Different types of fear-conditioned behaviour mediated by separate nuclei within amygdala. *Nature* **388**, 377–380 (1997).
15. Gore, F. *et al.* Neural representations of unconditioned stimuli in basolateral amygdala mediate innate and learned responses. *Cell* **162**, 134–145 (2015).
16. Paton, J.J., Belova, M.A., Morrison, S.E. & Salzman, C.D. The primate amygdala represents the positive and negative value of visual stimuli during learning. *Nature* **439**, 865–870 (2006).
17. Zirlinger, M., Kreiman, G. & Anderson, D.J. Amygdala-enriched genes identified by microarray technology are restricted to specific amygdaloid subnuclei. *Proc. Natl. Acad. Sci. USA* **98**, 5270–5275 (2001).
18. Namburi, P. *et al.* A circuit mechanism for differentiating positive and negative associations. *Nature* **520**, 675–678 (2015).
19. Heiman, M. *et al.* A translational profiling approach for the molecular characterization of CNS cell types. *Cell* **135**, 738–748 (2008).
20. Knight, Z.A. *et al.* Molecular profiling of activated neurons by phosphorylated ribosome capture. *Cell* **151**, 1126–1137 (2012).
21. Sanz, E. *et al.* Cell-type-specific isolation of ribosome-associated mRNA from complex tissues. *Proc. Natl. Acad. Sci. USA* **106**, 13939–13944 (2009).
22. Gay, L. *et al.* Mouse TU tagging: a chemical/genetic intersectional method for purifying cell type-specific nascent RNA. *Genes Dev.* **27**, 98–115 (2013).
23. Yang, Z., Edenberg, H.J. & Davis, R.L. Isolation of mRNA from specific tissues of *Drosophila* by mRNA tagging. *Nucleic Acids Res.* **33**, e148 (2005).
24. Lein, E.S. *et al.* Genome-wide atlas of gene expression in the adult mouse brain. *Nature* **445**, 168–176 (2007).
25. Hemmings, H.C. Jr., Greengard, P., Tung, H.Y. & Cohen, P. DARPP-32, a dopamine-regulated neuronal phosphoprotein, is a potent inhibitor of protein phosphatase-1. *Nature* **310**, 503–505 (1984).
26. Savander, V., Go, C.G., LeDoux, J.E. & Pitkänen, A. Intrinsic connections of the rat amygdaloid complex: projections originating in the basal nucleus. *J. Comp. Neurol.* **361**, 345–368 (1995).
27. Kantak, K.M., Black, Y., Valencia, E., Green-Jordan, K. & Eichenbaum, H.B. Dissociable effects of lidocaine inactivation of the rostral and caudal basolateral amygdala on the maintenance and reinstatement of cocaine-seeking behavior in rats. *J. Neurosci.* **22**, 1126–1136 (2002).
28. Choi, G.B. *et al.* Lhx6 delineates a pathway mediating innate reproductive behaviors from the amygdala to the hypothalamus. *Neuron* **46**, 647–660 (2005).
29. Root, C.M., Denny, C.A., Hen, R. & Axel, R. The participation of cortical amygdala in innate, odour-driven behaviour. *Nature* **515**, 269–273 (2014).
30. Peng, Y. *et al.* Sweet and bitter taste in the brain of awake behaving animals. *Nature* **527**, 512–515 (2015).
31. Aso, Y. *et al.* Mushroom body output neurons encode valence and guide memory-based action selection in *Drosophila*. *Elife* **3**, e04580 (2014).
32. Cohn, R., Morantte, I. & Ruta, V. Coordinated and Compartmentalized Neuromodulation Shapes Sensory Processing in *Drosophila*. *Cell* **163**, 1742–1755 (2015).
33. Duvarci, S. & Paré, D. Glucocorticoids enhance the excitability of principal basolateral amygdala neurons. *J. Neurosci.* **27**, 4482–4491 (2007).
34. Davis, M., Rainnie, D. & Cassell, M. Neurotransmission in the rat amygdala related to fear and anxiety. *Trends Neurosci.* **17**, 208–214 (1994).
35. Herry, C. & Johansen, J.P. Encoding of fear learning and memory in distributed neuronal circuits. *Nat. Neurosci.* **17**, 1644–1654 (2014).
36. Duvarci, S. & Pare, D. Amygdala microcircuits controlling learned fear. *Neuron* **82**, 966–980 (2014).
37. Tovote, P., Fadok, J.P. & Lüthi, A. Neuronal circuits for fear and anxiety. *Nat. Rev. Neurosci.* **16**, 317–331 (2015).
38. Janak, P.H. & Tye, K.M. From circuits to behaviour in the amygdala. *Nature* **517**, 284–292 (2015).
39. Parkinson, J.A., Robbins, T.W. & Everitt, B.J. Dissociable roles of the central and basolateral amygdala in appetitive emotional learning. *Eur. J. Neurosci.* **12**, 405–413 (2000).
40. Cai, H., Haubensak, W., Anthony, T.E. & Anderson, D.J. Central amygdala PKC-δ(+) neurons mediate the influence of multiple anorexigenic signals. *Nat. Neurosci.* **17**, 1240–1248 (2014).
41. Gallagher, M., Graham, P.W. & Holland, P.C. The amygdala central nucleus and appetitive Pavlovian conditioning: lesions impair one class of conditioned behavior. *J. Neurosci.* **10**, 1906–1911 (1990).
42. Knapska, E. *et al.* Differential involvement of the central amygdala in appetitive versus aversive learning. *Learn. Mem.* **13**, 192–200 (2006).
43. Knapska, E., Radwanska, K., Werka, T. & Kaczmarek, L. Functional internal complexity of amygdala: focus on gene activity mapping after behavioral training and drugs of abuse. *Physiol. Rev.* **87**, 1113–1173 (2007).
44. Han, S., Soleiman, M.T., Soden, M.E., Zweifel, L.S. & Palmiter, R.D. Elucidating an affective pain circuit that creates a threat memory. *Cell* **162**, 363–374 (2015).

ONLINE METHODS

Subjects. Wild-type C57BL/6J (stock #000664), mice were obtained from Jackson Laboratory. Cartpt-Cre mice (stock #036659-UCD), produced through the GENSAT project, were obtained from the Mutant Mouse Resource and Research Center (MMRRC). Cartpt-Cre mice were backcrossed to C57BL/6J for two generations. Rspo2-Cre mice were generated using a bacterial artificial chromosome (BAC) clone (RP32-39M21) with a Cre construct driven by the regulatory elements of *Rspo2*. Experiments were performed in mice 8–16 weeks of age. All subjects were male mice housed in a 12:12 h light cycle either in cohorts of 3–5 or, for postoperative animals, individually. All subjects were cared for and maintained in accordance with protocols approved by the Massachusetts Institute of Technology (MIT) Committee on Animal Care (CAC) and guidelines by the National Institutes of Health (NIH).

Viruses. The mouse minimal *Fos* promoter (−623 to +1050 from the transcriptional start site) followed by the advanced tetracycline transactivator, tTA, was cloned into an adeno-associated virus (AAV) backbone to generate the pAAV-Fos-tTA vector. A cDNA clone of mouse polyadenylate-binding protein 1, *Pabpc1*, with a C-terminal Myc-DDK tag (Origene, Cat. #MR209653), was subcloned into the tetracycline responsive element (*TRE*) backbone to generate the pAAV-TRE-PABP-Flag plasmid. AAV plasmids were packaged into AAV9 vectors by the Gene Therapy Center and Vector Core at the University of Massachusetts Medical School. AAV5-Ef1a-DIO-eArch3.0-eYFP (AV5257), AAV5-Ef1a-DIO-ChR2-eYFP (AV5226B), and AAV5-Ef1a-DIO-eYFP (AV4310D) were obtained from University of North Carolina at Chapel Hill Vector Core. AAV9-Ef1a-ChR2-eYFP (CS0633-3CS) was obtained from University of Pennsylvania School of Medicine Vector Core.

Stereotactic injections. Subjects undergoing stereotactic injections were anesthetized under isoflurane. Standard stereotactic procedures were used. Viruses were injected using a mineral oil–filled glass micropipette attached to a 1-µL microsyringe. For activity-dependent transcriptional profiling, 200 nL of ~2.0 × 10⁹ GC of AAV9-cfos-tTA and AAV9-TRE-Pabpc1-Flag (1:1 mixture) were bilaterally injected into the BLA (distance from bregma, AP −1.4 mm, ML ±3.3 mm, DV −4.85 mm) of doxycycline (Dox)-fed mice and incubated for 7 d before downstream experiments. For behavioral experiments, 200 µL of viral stocks of AAV5 Cre-dependent viruses was injected into the BLA of Rspo2-Cre (AP −1.6 mm, ML ±3.3 mm, DV −4.85 mm) and Cartpt-Cre mice (AP −2.0 mm, ML ±3.4 mm, DV −4.9 mm) and incubated for 3–4 weeks before behavioral experiments. For retrograde tracing, Alexa Fluor 555–conjugated cholera toxin subunit B (CTB) (1 µg/µL) was unilaterally injected into the NAc (300 nL, AP +1.0 mm, ML +0.75 mm, DV −4.8 mm), CeM/CeL (100 nL, AP −1.35 mm, ML +2.9 mm, DV −4.7 mm) or CeC (100 nL, AP −1.0 mm, ML +2.9 mm, DV 4.3 mm) and incubated for 7 d before sacrifice. Dual CTB (CTB-Alexa 555 and CTB-Alexa 647) was injected into the PL (AP −1.75 mm, ML +0.3 mm, DV −2.3 mm) and IL (AP −1.6 mm, ML +0.3 mm, DV −2.6 mm) and incubated for 7 d before sacrifice. For brain slice electrophysiological experiments, 200 nL of AAV9-Ef1a-DIO-ChR2-eYFP was injected into the BLA of Rspo2-Cre and Cartpt-Cre mice 4–5 weeks old and incubated 4 d before electrophysiological experiments.

Fiber implantation. Mono fiber optic cannulas (5.0 mm, Doric Lens) were implanted (unilaterally or bilaterally, depending on the experiment) above the BLA of Rspo2-Cre and Cartpt-Cre (AP −2.0 mm, ML +3.3 mm, DV −4.3 mm), and above the NAc of Rspo2-Cre (AP +1.3 mm, ML +0.75 mm, DV −4.0 mm). Once positioned above the BLA, the mono fiber optic cannula was cemented using dental cement (Teets Cold Cure; A-M Systems) to the skull, which contained two screws that lay medially to the implant site. Once the dental cement cured, a protective cap surrounding the implant, made using a 1.5 mL black Eppendorf tube, was fixed onto the implant using dental cement. Mice spent 3–4 week post-operation for recovery. Mice were handled by the investigator 2–3 d before behavioral experiments.

RNA immunoprecipitation. Twelve wild-type male mice kept on Dox diets were bilaterally injected with AAV9-Fos-tTA and AAV9-TRE-Pabpc1-Flag virus. One week after operation, mice were taken off the Dox diet for 2 d and underwent a fear conditioning protocol (three shocks, 0.75 mA, 2 s duration) (shock group) or exposure to a female mouse in the home cage for 2 h (female group). Immediately after, mice were returned to a Dox diet. Two days later, mice were anesthetized with isoflurane and were sacrificed by decapitation. Two control mice were kept on a Dox diet. Brains were dissected, flash frozen on dry ice, and stored at −80 °C until RNA immunoprecipitation. Mice undergoing histological analysis underwent either fear conditioning or reward conditioning off Dox (as described above), in addition to kainic acid–induced seizure (20 mg/kg kainic acid) or home cage, before paraformaldehyde fixation (described below). RNA immunoprecipitation was performed in a similar fashion to that described by the McKnight laboratory (University of Washington)[20]. Brains were thawed for 30 min in a −16 °C cryostat; 300-µm sections across the BLA were collected. Using a razor blade, the BLAs were crudely dissected from two mouse brains and were collected into a single 1.5-mL microcentrifuge tube. This yielded ~30 µg of brain tissue. One milliliter of homogenization buffer (HB, 1% NP-40, 100 mM KCl, 50 mM Tris pH 7.4, 12 mM MgCl₂, 200 U/mL Promega RNasin, 1 mM DTT, 100 µg/mL cycloheximide, 1 mg/mL heparin, 1% protease inhibitors (P8340, Sigma)) was added. Samples were transferred to a 2-mL Dounce homogenizer and homogenized using pestle A and, subsequently, pestle B. Homogenized samples were transferred to 1.5-mL microcentrifuge tubes and were centrifuged at 10,000g. Supernatant was separated into a new microcentrifuge tube and 5 µL of anti-Flag (F7425, Sigma) was added and incubated for 6 h at 4 °C. 200 µL Pierce A/G Magnetic Beads were washed in HB, added to the homogenates, and incubated overnight at 4 °C. Magnetic beads were separated using a magnetic tube rack and washed three times in a salt buffer (0.3 M KCl, 1% NP-40, 50 mM Tris pH 7.4, 12 mM MgCl₂, 100 µg/mL cycloheximide, 0.5 mM DTT). Protein–RNA complexes were dissociated from magnetic beads by vortexing samples in lysis buffer (RLT lysis buffer from Qiagen RNeasy kits with 10 µL/mL β-mercaptoethanol). Magnetic beads were drawn off and RNA was isolated using the Qiagen RNeasy Micro Kit. RNA samples were stored at −80 °C until further experiments.

RNA analysis. RNA samples were analyzed using the Affymetrix Mouse 430 2.0 chip by MIT BioMicroCenter. CEL files from the Mouse 430 2.0 chip were normalized by RMA or MAS5 through the Affymetrix Expression Console Software. Subsequently, CHP files were analyzed through Affymetrix Transcriptome Analysis Console 2.0; three samples from the shocked mice and three samples from the female-exposed mice were grouped. The data from this analysis have been deposited to the NCBI Gene Expression Omnibus (GEO), accession code GSE78137.

Screening and selecting BLA gene marker candidates. On the basis of the data obtained from the array, the top gene candidates, independent of statistical significance, enriched in either the RMA or MAS5 normalized data set were screened on the Allen Mouse Brain Expression Atlas (http://mouse.brain-map.org/)[24]. On the basis of expression patterns in the shock group, 16 gene candidates that were enriched in the shock group were selected: *Acvr1c*, *Cdh9*, *Crhbp*, *Gabra1*, *Gabra2*, *Gria4*, *Htr2c*, *Htr3a*, *Nptx2*, *Nrxn3*, *Pthlh*, *Pcdh18*, *Rspo2*, *Sema5a*, *Slc30a1*, *Zfpm2*. On the basis of expression patterns in the BLA, 21 gene candidates that were enriched in the female group were selected: *Adrbk1*, *Aig1*, *Esrra*, *Gipc1*, *Gpr39*, *Gpr137*, *Gpr165*, *Gria1*, *Grin1*, *Oprl1*, *Neurl1a*, *Nos1*, *Nos1ap*, *Ntrk3*, *Ntng2*, *Penk*, *Ppp1r1b*, *Slc24a4*, *Slc30a3*, *Stx1a*, *Synpo*. Interneuronal markers—*Calb1*, *Npy*, *Sst*, *Vip*, *Pvalb*—and pyramidal cell markers—*Camk2a*, *Thy1*—were selected as positive controls.

Tissue. For screening candidate gene markers, wild-type mice 12–16 weeks old were anesthetized with isoflurane and were sacrificed by decapitation. Brains were quickly dissected and immediately flash frozen on aluminum foil on dry iced and stored at −80 °C. A single session of sectioning consisted of 12 wild-type brains and 60 Superfrost Plus slides (25 × 75 mm, Fisherbrand). Thirty minutes before sectioning, brains were equilibrated to −16 °C in a cryostat. Brains were serially sectioned coronally at 20 µm and thaw-mounted onto slides. Each mouse brain produced one section on each of 60 slides—sections from AP −0.8 mm to AP −2.0 mm were taken from each brain. Sections from each subsequent brain started in a staggered fashion (begun on the 6th, 11th, 16th, etc. slide). Therefore, each slide resulted in 12 coronal brain sections representing 0.1 mm intervals between AP −0.8 mm and AP −2.0 mm. Brains were dried at room temperature for 30 min before storage at −80 °C. In order to obtain a homogenous representation of the BLA, we allowed the loss of no more than two sections during sectioning of a single brain.

For single-molecule fluorescence *in situ* hybridization, mouse brains were collected through the flash freezing method (as described above). Using a cryostat, an individual brain was serially sectioned and thaw-mounted onto Superfrost Plus slides. Coronally cut brain slides were serially sectioned at 20 µm onto 10 slides, each slide containing 11 or 12 brain sections, spaced 0.2 mm apart spanning AP −0.8 mm to AP −2.8 mm. Sagittally cut brain slides was serially sectioned at 20 µm onto 8 slides, each slide containing at least 12 brain sections, spaced 0.16 mm apart spanning ML 3.8 mm to ML 2.8 mm. Slides were dried at room temperature for 60 min before storage at −80 °C.

For immunohistochemistry, mice were euthanized by Avertin overdose and perfused with phosphate-buffered saline (PBS) and 4% paraformaldehyde. Brains were dissected and stored in 4% paraformaldehyde at room temperature for 8 to 12 h, before storage in PBS at 4 °C. Coronally cut brains were sectioned at 50 µm on a vibratome and serially collected into four wells. Each well contained coronal sections spaced 0.2 mm apart.

Fluorescence *in situ* hybridization. Single-label fluorescence *in situ* hybridization (FISH) was performed using RNA probes generated from the pCRII-TOPO Vector (ThermoFisher). pCRII-TOPO vector, cut with EcoRI, was used as the backbone for cloning cDNA of candidate gene markers. Mouse brain cDNA was obtained via reverse transcription using the Omniscript RT kit (Qiagen) on RNA extracted from mouse brains (Qiagen RNeasy Lipid Tissue Mini Kit). PCR primers were the same as the forward and reverse primers reported on Allen Mouse Brain Expression Atlas[24] with the addition of 5′-CAGTGTGCTGGAATT-3′ and 5′-GATATCTGCAGAATT-3′ to the 5′ end of the forward primer and reverse primer, respectively. PCR products for each candidate gene was isolated and cloned into the pCRII-TOPO backbone using TOPO cloning (Clontech In-Fusion HD) and maintained in Stellar Competent Cells (Clontech). RNA probes were generated by cutting pCRII-TOPO plasmids with HindIII and transcribing the antisense strand using a T7 RNA polymerase (NEB, HiScribe T7 High Yield RNA Synthesis Kit) with digoxigenin-labeled UTP (Roche). Digoxigenin-labeled antisense RNA probes were isolated (Qiagen, RNeasy Mini Kit) and stored at −80 °C.

Tissue preparation for single-label FISH was performed similarly to standard mouse brain FISH protocols. On day 1, slides were fixed in 4% paraformaldehyde at 4 °C, washed twice in phosphate buffer pH 7.4, rinsed in diethylpyrocarbonate (DEPC) water and triethanolamine (TEA) buffer, pretreated with acetic anhydride, washed in 2× saline-sodium citrate solution (SSC), washed in increasing concentrations of ethanol (70%, 95%, 100%), delipidated with chloroform, and washed with decreasing concentrations of ethanol (100%, 95%). The probes were dried for 2 h at room temperature. RNA probes were denatured at 100 °C and cooled on ice, then were applied to slides in a solution of hybridization buffer and tRNA and coverslipped for overnight incubation at 60 °C. On day 2, slides underwent post-hybridization stringency washes—2× saline-sodium phosphate-EDTA buffer (SSPE), 50% formamide in 2× SPPE at 60 °C, and twice in 0.1× SSPE at 60 °C. Endogenous peroxidase activity was removed with 0.3% hydrogen peroxide in Tris-NaCl-Tween (TNT) buffer, followed by three washes in TNT buffer. Slides were blocked in TNT buffer with blocking reagent (PerkinElmer) (TNB) before being incubated with 1:100 peroxidase-conjugated anti-digoxigenin FAB fragment (anti-dig-POD, Roche) for 2 h at room temperature. Anti-dig-POD was removed by a series of three TNT washes. Alexa 594–conjugated tyramide signal amplification (TSA) solution was applied over the slides for 30 min and then washed away with a series of three TNT washes. Slides were coverslipped and mounted using VectaShield mounting solution containing DAPI (Vector Laboratories).

Percent labeling was calculated as the number of RNA-positive cells as a percentage of the total large (<10 µm) DAPI⁺ BLA cells, which is an indirect indicator of BLA principal cells as shown from quantification of *Camk2a*⁺ cells (**Fig. 1l**).

Single-molecule fluorescence *in situ* hybridization. Single molecule fluorescence *in situ* hybridization (smFISH) was performed using a RNAscope Fluorescent Multiplex Kit (Advanced Cell Diagnostics). Custom C1 and C2 DNA oligonucleotide probes were designed for *Rspo2* and *Ppp1r1b*. *Camk2a* and *Gad1* probes were purchased from the Advanced Cell Diagnostics catalog. Brain sections were fixed in 4% paraformaldehyde for 15 min and then washed in 50%, 70%, 100%, and 100% ethanol for 5 min each. Slides were dried for 5 min. Proteins were digested using protease solution (pretreatment solution 3) for

60–90 s on wild-type tissues, 30 s on CTB-expressing tissues, and 5–10 s on eYFP-expressing tissues. Immediately afterward, slides were washed twice in PBS. In parallel, C1 and or C2 probes were heated in a 40 °C water bath for 10 min. Probes were applied to the slides, which were coverslipped and placed in a 40 °C humidified incubator for 3 h. Slides were rinsed twice in RNAscope wash buffer and then underwent the colorimetric reaction steps according to standard kit protocol using AMP4A (C1, green; C2, red) or AMPB (C1, red; C2, green) depending on the color combination of choice. After the final wash buffer, slides were immediately coverslipped using ProLong Diamond Antifade mounting medium with DAPI (ThermoFisher).

Immunohistochemistry. Free floating brain sections were washed in PBST (PBS, 3% TritonX) three times for 10 min, blocked for 1 h in blocking buffer (PBST, 5% normal goat serum), and incubated in primary antibody in blocking buffer overnight at 4 °C. On the next day, brains were washed with three 10-min washes of PBST and incubated in secondary antibody in blocking buffer at room temperature for 2 h. Primary antibodies used were rabbit anti-Flag (F7425, Sigma, 1:1,000), chicken anti-GFP (Invitrogen, A10262, 1:1,000) and rabbit anti-Fos (Santa Cruz, sc-52, 1:2,000). Secondary antibodies used were goat anti-chicken Alexa Fluor 488 (Invitrogen, A11039, 1:1,000) and goat anti-rabbit Alexa Fluor 555 (Invitrogen, A21428, 1:1,000). After three more 10-min PBST washes, slides were coverslipped and mounted using VectaShield mounting solution containing DAPI (Vector Laboratories).

For immunohistochemistry of brains subjected to electrophysiological experiments, brain slices were washed in PBST three times for 10 min, blocked for 1 h, and then incubated overnight at 4 °C with chicken anti-GFP (Invitrogen, A10262, 1:1,000) to visualize ChR2-eYFP fibers and CF555 streptavidin (Biotium, 29038, 1:100) to visualize recorded neurons. On the next day, slices were washed in PBST three times for 10 min, and then incubated in chicken anti-GFP (Invitrogen, A10262, 1:1,000) for 2 h at room temperature. After three more 10-min PBST washes, slides were dried at room temperature for at least 6 h before coverslipping and mounting using VectaShield mounting solution containing DAPI (Vector Laboratories).

Microscopy and histological representation. Micrographs were obtained using a Zeiss fluorescent microscope or Zeiss AxioImager M2 confocal microscope using Zeiss ZEN (black edition) software. Main figure representations were colored green for *Rspo2*⁺ neurons and red for *Ppp1r1b*⁺ irrespective of native fluorescent labeling.

c-Fos experiment. Wild-type mice were handled by investigator once each day for 3 d before stimulus exposure. Stimulus exposure experiments occurred within 1 h of the dark cycle. Shocked mice were exposed to a fear conditioning chamber (Med Associates) for 500 s and received three footshocks (0.75 mA, 2 s duration), then returned to the home cage, where water and food were removed. Female-exposed mice were transported in home cages to an experimental room and were exposed to a wild-type female mouse. Context-exposed mice were exposed to the fear conditioning chamber for 500 s then returned to the home cage, where water and food were removed. Odor-exposed mice were transported in home cages to an experimental room; water and food were removed, and the mice were habituated for 4 h before odor exposure. One milliliter of TMT (10% TMT in dH₂O), 1 mL of peanut oil, or 1 mL of benzaldehyde (0.25% in 70% ethanol) were pipetted into the center of the home cage. Water-deprived (overnight) wild-type mice were transported in home cages to an experimental room, food removed, and habituated for 4 h before hydration. A bottle of water, quinine water (0.05% quinine hydrochloride dihydrate), sucrose water (5% sucrose), or an empty water bottle without a spout was placed into the home cage. Ninety minutes after initial exposure, mice were sacrificed using Avertin overdose and perfused for immunohistochemical analysis of c-Fos. For smFISH of *Fos*, mice underwent the same stimulus exposure protocol but were sacrificed using the flash freezing method (described above) 15 min after the end of the stimulus exposure or, in the case of water exposure, 15 min after satiety, which took <5 min after water exposure. Background signals levels of c-Fos and *Fos* plus *Rspo2* or *Ppp1r1b* were adjusted in ZEN and were exported into image files for quantification in a blind fashion. The relative *Fos* expression for the aBLA was calculated by (number of *Fos*⁺ cells in the aBLA)/(total number of *Fos*⁺ cells in the BLA); likewise, that in the pBLA was calculated by (number of *Fos*⁺ cells in the pBLA)/(total number of *Fos*⁺

cells in the BLA). The aBLA and pBLA were determined using mouse brain atlas boundaries (**Supplementary Fig. 4**). The relative *Fos* expression of the aBLA and pBLA are mutually exclusive. Thus, when statistically comparing values between different conditions, significance values for comparison of the aBLA and comparison of the pBLA were redundant. Because of this, only the statistics for the aBLA are graphically represented (**Fig. 3d–f**). IHC c-Fos counting was performed for unilateral BLAs on 50-μm sections. smFISH *Fos* counting was performed for unilateral BLAs on three 20-μm sections per mouse. The AP position was determined by a mouse brain atlas and was accurate within ± 0.2 mm.

For the *Fos* experiments in **Figure 6**, Ppp1r1b-ChR2 and Ppp1r1b-eYFP mice (**Fig. 5g–i**) were exposed to three footshocks in a similar manner, but simultaneously with footshocks received a 10-s, 20-Hz train of 15-ms pulses at 473 nm bilaterally to the BLA. Water-deprived (overnight) Rspo2-ChR2 and Rspo2-eYFP mice (**Fig. 5j–l**) were exposed to water in a similar manner to that described in above in the wild-type experiments, but manually (by the experimenter) received a 20-Hz train of 15-ms pulses at 473 nm bilaterally to the BLA contingent on drinking water. Thirty minutes after end of the stimulus exposure or, in the case of water exposure, 30 min after satiety, which took <5 min after water exposure, mice were sacrificed using the flash freezing method (described above). Background signals levels of *Fos* and *Fos* plus *Rspo2* or *Ppp1r1b* were adjusted in ZEN and were exported into image files for quantification in a blind fashion. Three sections of *Fos* plus *Rspo2* or *Ppp1r1b* per mouse brain were quantified in a blind fashion.

Fear conditioning. On day 1, mice were placed in to a fear conditioning chamber (Med Associates) while bilaterally connected to optic fiber patch cords (Doric Lens) for 500 s and received footshocks at the 198-s, 278-s and 358-s time points. For optical inactivation experiments, simultaneously with the footshocks at the 198-s, 278-s and 358-s time points, a constant pulse of 532-nm light (10–15 mW) was delivered through the optical cannulas for duration of 20 s; for optical activation experiments, a 10-s, 20-Hz train of 15-ms pulses of 473-nm (10–15 mW) light was used. On day 2, mice were connected to optic fiber patch cords and placed in the fear conditioning chamber for 180 s, where no shock or laser was delivered. Freezing behavior was scored manually using JWatchers1.0 in a blind fashion. Freezing was scored (**Fig. 4c**) on day 1 from the onset of the first shock to the end of the trial and day 2 from the beginning to end of the trial. Freezing scored in bins (**Fig. 5b**) was binned on day 1 from the start of the fear conditioning trial to the first shock (198 s), then subsequently between the inter-shock intervals (80 s). On day 2, the 3 min test, freezing was binned into three bins (1 min).

Reward conditioning. Water-restricted mice were placed in an operant conditioning chamber (Island Motion) with one reward port equipped with a cue light. At the start of each trial, the onset of the cue light signaled the availability of water reward contingent on a nose poke, lasting 5 s. Upon a successful nose-poke any time during the 5 s, a reward was immediately delivered through a water spout in the port and the cue light was turned off. A TTL triggering a laser pulse, bilaterally delivered to the implanted optic cannula, was issued at the same time as the reward delivery. For optical inactivation experiments, a constant 10-s pulse of 532-nm light (10–15 mW) was used; for optical activation experiments, a 10-s, 20-Hz pulse train of 15-ms pulses of 473-nm light (10–15 mW) was used. During the following inter-trial interval, randomly distributed between 10 and 15 s, nose pokes did not elicit water rewards. Timestamps for cue light, nose pokes and reward deliveries were logged and analyzed with Matlab. Data arrays were constructed from the first rewarded trial to 150 trials thereafter. Total number of pokes was counted for the period. Percent in-port time during the cue presentation were calculated in 100-ms time bins and quantified with a *z*-score procedure ($z = (x - \mu)/\sigma$), where *x* is the average percent time spent in the reward port and μ and σ are the mean and s.d. of percent time spent in the reward port during the 5 s baseline period before cue onset.

Optogenetic freeze test. On day 1, mice were placed in a fear conditioning chamber for 360 s. 20-Hz, 473-nm light (10–15 mW) was unilaterally delivered through the optic cannula at the 180-s time point for 180 s. On day 2, mice were connected to fiber optic patch cords and returned to the fear conditioning chamber for 180 s without light stimulation. Freezing behavior was scored manually using JWatchers1.0 in a blind fashion.

Optogenetic self-stimulation test. On day 1, food-deprived mice were placed into an operant conditioning chamber (Med Associates) equipped with a single nose port. The nose port contained a single food pellet to attract the mouse to the port. 20-Hz, 473-nm light (10–15 mW, 5 s duration) was unilaterally delivered through the optic cannula contingent on a beam break in the nose port. Mice spend a total of 1 h in the operant chamber. On day 2, mice were connected to fiber optic patch cords and returned to the reward conditioning chamber (with no food pellet) for 15 min without light stimulation. Total number of pokes was quantified by MED-PC (Med Associates) software on day 1 and day 2.

Optogenetic place preference test. Mice were placed into the center of a rectangular box (70 × 25 × 31 cm) where each end of the box contained distinct wall cues. Immediately upon entry into the box, mice received continuous 20-Hz, 473-nm light stimulation (10–15 mW) contingent on entry into a randomly preselected half of the box for 5 min. Each mouse ran two trial 1 h apart, in which the side of stimulation was counterbalanced. The average difference score was take from both trials. The position of the mice was tracked using EthoVision XT video tracking software (Noldus). The difference score was calculated by (duration in the stimulated side) – (duration in the non-stimulated side).

All behavioral experiments were performed by a set of mice in cohorts of 4–16 mice and initiated within 2 h of the onset of dark cycle. Animals were selected for surgery and behavior in a pseudorandom fashion in that mice were, as much as possible, divided equally on the basis of age and parents into experimental and control groups. Groups of mice did not undergo multiple behavioral assays. For unilateral implants, mice received implants randomly and in a counterbalanced manner in the left or right hemisphere. For all behavioral experiments, two-tailed unpaired Student's *t*-tests were performed between experimental groups and control groups. Mice lacking expression or misplaced fibers were excluded from analysis. Experimenters were blind during data analysis and whenever possible during the experimentation.

Optogenetic slice electrophysiology. Male mice (mean-PND 45 d) were anesthetized by isoflurane and their brains were dissected. Using a vibratome (VT1000S, Leica), we prepared 300-μm-thick parasagittal slices containing the basolateral amygdala in oxygenated cutting solution at ~4 °C. Slices were then incubated at ~23 °C in oxygenated artificial cerebrospinal fluid (ACSF). The cutting solution contained 3 mM KCl, 0.5 mM $CaCl_2$, 10 mM $MgCl_2$, 25 mM $NaHCO_3$, 1.2 mM $NaHPO_4$, 10 mM D-glucose, 230 mM sucrose, saturated with 95% O/5% CO (pH 7.3, osmolarity 340 mOsm). The ACSF contained 124 mM NaCl, 3 mM KCl, 2 mM $CaCl_2$, 1.3 mM $MgSO_4$, 25 mM $NaHCO_3$, 1.2 mM $NaHPO_4$, 10 mM D-glucose, saturated with 95% O/5% CO (pH 7.3, osmolarity 300 mOsm). Slices were transferred to a submerged experimental chamber and perfused with oxygenated 36 °C ACSF at a rate of 3 ml min^{-1}.

Whole-cell recordings in current-clamp or voltage-clamp mode were performed by using an infrared differential interference contrast microscope (BX51, Olympus) with a water immersion 40× objective (N.A. 0.8), four automatic manipulators (Luigs & Neumann) and a CCD camera (Orca R2, Hamamatsu). Borosilicate glass pipettes were fabricated (P97, Sutter Instrument) with a resistances of 3–5 MΩ and filled with the following intracellular solution: 110 mM potassium gluconate, 10 mM KCl, 10 mM HEPES, 4 mM ATP, 0.3 mM GTP, 10 mM phosphocreatine and 0.5% biocytin (pH 7.25, osmolarity 290 mOsm). Recordings in voltage clamp mode were performed by using the following intracellular solution (in mM): 117 cesium methansulfonate, 20 HEPES, 0.4 EGTA, 2.8 NaCl, 5 TEA chloride, 4 Mg-ATP, 0.3 Na-GTP, 10 QX314, 0.1 spermine and 0.5% biocytin (pH 7.3, osmolarity 290 mOsm). Access resistance was monitored throughout the duration of the experiment and data acquisition was suspended whenever the resting membrane potential was depolarized above −50 mV or the access resistance was beyond 20 MΩ. Recordings were amplified using up to two dual-channel amplifiers (Multiclamp 700B, Molecular Devices), filtered at 2 kHz, digitized (20 kHz) and acquired using custom software running on Igor Pro (Wavemetrics). Software and code are available upon request. Gabazine was obtained from Tocris.

Optogenetic stimulation was achieved through a 460-nm LED light source (XLED1, Lumen Dynamics) driven by TTL input with a delay onset of 25 μs (subtracted offline). Light power on the sample was 33 mW mm^{-2}, and only the maximum power was employed. Slices were stimulated by single 2-ms light pulse repeated 20 times every 4 s or train of 15 light pulses at 10 Hz repeated 20 times

every 6 s. In voltage-clamp mode cells were held at −70 mV for EPSC measurement and at 0 mV for IPSC measurements, whereas in current mode EPSPs, IPSPs and action potentials were measured at resting potentials.

The intrinsic electrophysiological properties were measured current mode with the cell held at −70 mV. Input resistance was estimated by linear fit of the *I-V* relationship (injection of 10–12 current steps of 1-s duration). Action potential threshold was tested with a current ramp injection. Membrane time constant was estimated by single exponential fit of the recovery time from a −100 pA current step injection of 1 s duration. Synaptic connections, in voltage or current mode, were determined by averaging 20 trials. EPSC amplitude was measured from the average maximum peak response by subtracting a baseline obtained 5 ms before light pulse starts. EPSC onset was measured from the beginning of the light pulse to the starting point of the response estimated through the intercept between the baseline and a parabolic fit of the rising phase of the EPSC. To compute the probability of connection (*n* successes/*n* tests) we used only slices with reliable ChR2 expression characterized at least by one responsive postsynaptic cell (principal cell or interneuron).

Statistical analysis was performed using Igor (Wavemetrics), GraphPad (Prism), or Excel (Microsoft). The distribution of the data was tested with the Kolmogorov-Smirnov test and a two-tailed paired or unpaired *t*-test or a Wilcoxon signed-rank or rank-sum test was employed accordingly. A Fisher exact test was employed to verify the significance of the connection probability. Data are presented as mean ± s.e.m.

As the recorded cells were filled with biocytin, slices were recovered and fixed in 4% paraformaldehyde for morphological identification.

Single-cell quantitative polymerase chain reaction. In wild-type mouse brain slices, at the end of the patch clamp recordings, the cytoplasm of the recorded neuron was collected by applying negative pressure to the recording pipette. Once the cytoplasmic contents were suctioned, the glass pipette was quickly transferred to a 0.2-mL PCR tube filled with 10 μL RNase-free water, 2 μL oligo(dT), 1 μL dNTP, 1 μL RNaseOUT provided by the SuperScript III CellsDirect cDNA Synthesis Kit (ThermoFisher). Samples were placed on a 70 °C heat block for 5 min, and then chilled on ice. For first strand synthesis, 8 μL of RT mix was added to the sample (6 μL 5× RT Buffer, 1 μL 0.1 M DTT, 1 μL Superscript III RT) and incubated on a 50 °C heat block for 50 min. After the first strand synthesis, reverse transcriptase was inactivated by 5 min incubation on an 85 °C heat block. Samples were stored at −20 °C until quantitative polymerase chain reaction (qPCR).

qPCR was performed using the TaqMan Gene Expression Assays (Applied Biosystems). The genetic identity of BLA neuron using qPCR was determined by the ratio between *Rspo2* and *Ppp1r1b* expression. The qPCR reaction consisted of 25 μL 2× TaqMan Gene Expression Master Mix, 2.5 μL 20× TaqMan Gene Expression Assay for *Rspo2* (Mm00555790_m1) or *Ppp1r1b* (Mm00454892_m1), 7 μL of cDNA template, and 17.5 μL of RNase free water. qPCR reaction was performed in an Applied Biosystems 7500 Real-Time PCR System using the fluorescein (FAM) channel with the standard qPCR reaction protocol for 60–80 cycles. The majority of cells did not result in amplification of either *Rspo2* or *Ppp1r1b*. Therefore, *Rspo2*^{+} and *Ppp1r1b*^{+} neurons were identified on the basis of the criterion of positive amplification. *Rspo2*^{+} or *Ppp1r1b*[+] amplification appeared at threshold cycles (CT) <50 cycle for most cells (**Fig. 1f**). qPCR-confirmed (*Rspo2*^{+} and *Ppp1r1b*[+]) and unconfirmed (magnocellular and parvocellular) neurons were statistically compared (**Table 1**). qPCR-confirmed *Rspo2*^{+} and *Ppp1r1b*^{+} neurons were not statistical different from unconfirmed, magnocellular and parvocellular neurons, respectively. Therefore, *Rspo2*^{+} and *Ppp1r1b*^{+} neurons were identified in the **Figure 6** experiment using a combination of soma diameter, AP distance from bregma, resistance, and capacitance (**Fig. 6k–n**)

Statistical analysis. Statistical analysis and statistical graphics was generated using GraphPad Prism 6.0. No statistical methods were used to predetermine sample sizes, but our sample sizes and statistical tests were determined on the basis of and were similar to those in previous studies examining similar behaviors and histology analyses[10,29]. Data distribution was assumed to be normal on the basis of similar measurements from previous literature but this was not formally tested for all statistical tests[10,29]. Variance was not significantly different between groups that were compared and met the assumptions of the statistical tests with the exception from groups where the effects of experimental manipulations were dramatic, such as in the case of Rspo2-ChR2 vs. Rspo2-eYFP in the optogenetic freeze test or Ppp1r1b-ChR2 vs. Ppp1r1b-eYFP in the optogenetic self-stimulation test. All data are represented as mean ± s.e.m. All *t*-test and ANOVA analyses were two-sided. A **Supplementary Methods Checklist** is available.

Data availability. Data available upon request. RNA microarray data may be found on NCBI Gene Expression Omnibus (GEO), accession code GSE78137.